HOKKAIDO UNIVERSITY

Title	Establishment and Pathology of a Murine Model of Influenza Virus-Associated Encephalopathy
Author(s)	Tanaka, Tomohisa; 田中, 智久
Degree Grantor	北海道大学
Degree Name	博士(獣医学)
Dissertation Number	甲第9486号
Issue Date	2010-03-25
DOI	https://doi.org/10.14943/doctoral.k9486
Doc URL	https://hdl.handle.net/2115/42819
Type	doctoral thesis
File Information	tanaka_thesis.pdf

Establishment and Pathology of a Murine Model of Influenza Virus-Associated Encephalopathy

インフルエンザ脳症マウスモデルの確立と病態解析

Tomohisa Tanaka

Laboratory of Comparative Pathology, Department of Veterinary Clinical Sciences, Graduate School of Veterinary Medicine, Hokkaido University

Contents

List of Abbreviations

BBB	blood-brain barrier
CNS	central nervous system
COX	cyclooxygenase
CSF	cerebrospinal fluid
DAB	3, 3'-diaminobenzidinetetrahydrochloride
DIC	disseminated intravascular coagulation
dpi	days post infection
EB	Evans Blue
GFAP	glial fibrillary acidic protein
HE	hematoxylin-eosin
IAE	influenza virus-associated encephalopathy
IAV	influenza A virus
IFN	interferon
IHC	immunohistochemistry
IL	interleukin
LPS	lipopolysaccharide
PBS	phosphate buffered saline
PFU	plaque forming units
SDS-PAGE	sodium dodecyl sulfate-polyacrylamide gel electrophoresis
SEM	standard error of the mean
TdT	terminal deoxynucleotidyl transferase
TJ	tight junction
TLR	Toll-like receptor
TNF	tumor necrosis factor
TUNEL	terminal deoxynucleotidyl transferase-mediated dUTP nick end-labeling
ZO-1	zona occludens-1

General Introduction

Influenza virus-associated encephalopathy (IAE) is a rare but highly lethal neural complication of influenza virus infection. IAE mostly affects children, with 80% of afflicted individuals younger than 5 years of age, and a peak incidence among children aged 1-2 years (Morishima *et al*, 2002). Death occurs in approximately 30% of patients and neurological defects are observed in about 30% of the surviving IAE cases (Smidt *et al*, 2004). The disease is highly prevalent in Japan, where there are approximately 100 cases of IAE every flu season. The disease does not appear to be unique to Japan, as cases closely resembling IAE have been reported in other countries (Chen *et al*, 2005; Huang *et al*, 2003; Newland *et al*, 2007; Toovey, 2008; Weitkamp *et al*, 2004). Although the role of genetic factors and the immature nature of the blood-brain barrier (BBB) have been postulated as underlying factors, it is unclear why IAE is so prevalent in Japanese children. IAE is typically associated with H3N2 influenza A virus (IAV) infection (Morishima *et al*, 2002; Togashi *et al*, 2004). Nearly 90% of IAE cases are associated with H3N2 IAV infection; the remaining 10% are associated with H1N1 IAV and influenza B virus. Most recently, cases of IAE associated with the 2009 pandemic H1N1 virus have been reported in Japan and other countries (Centers for Disease Control and Prevention, 2009).

The characteristic clinical course of IAE is an abrupt onset of seizure and coma within 24-48 hours (h) of the development of high fever (Morishima *et al*,

2002). Post-mortem pathological analysis typically reveals symmetrical vasogenic brain edema with hyalinization of blood vessels and extravascular hyaline droplet formation in the brain (Morishima *et al*, 2002; Togashi *et al*, 2004). This microscopic finding means disruption of the BBB due to damage to blood vessels, followed by influx of plasma component into cerebral parenchyma and the resultant encephalopathy. IAE is often followed by disseminated intravascular coagulation (DIC) and multiple organ failure, probably due to systemic endothelial cell damage (Togashi *et al*, 2004; Yokota *et al*, 2000). These clinical findings suggest that the essential component of IAE is damage to vascular endothelial cells (Morishima *et al*, 2002). The abrupt onset and rapid progression of IAE in young children makes early diagnosis of the disease difficult. Treatment of IAE is also difficult, as the exact pathological mechanism is unknown. In most IAE patients, influenza virus is recovered only from mucosal epithelial cells of the respiratory tract. Isolation of the virus from the central nervous system (CNS), including the brain and cerebrospinal fluid (CSF), is rare (Ito *et al*, 1999; Smidt *et al*, 2004). Neither viral antigen nor viral genome is detected in the brain by immunohistochemistry (IHC) (Togashi *et al*, 2004). Thus, direct invasion of the CNS by influenza virus is considered irrelevant as a cause of IAE. Elevated concentrations of several cytokines, including tumor necrosis factor (TNF)-α, soluble TNF receptor 1, interleukin (IL)-6, and IL-1β, have been reported in serum and CSF of IAE patients (Ichiyama *et al*, 2003; Ito *et al*, 1999). The concentrations of these inflammatory cytokines correlate with the severity of CNS dysfunction

2

(Aiba *et al*, 2001; Toovey, 2008). Thus, hypercytokinemia is believed to play an important role in the development of IAE. However, it is unclear whether hypercytokinemia causes or is a result of IAE, since the role of hypercytokinemia in IAE has yet to be experimentally confirmed. As such, the direct cause of hypercytokinemia in IAE is unknown. Administration of selective cyclooxygenase-2 (COX-2) inhibitors, such as diclofenac, has been reported to increase the mortality rate of IAE. Inhibition of COX-2, an inducible enzyme responsible for the formation of prostanoids (Diaz *et al*, 1998), is believed to exacerbate the vascular endothelial cell damage in IAE. Inhibition of COX-2, therefore, is a possible pathogenic factor in IAE. Blood coagulation abnormalities are sometimes observed in patients with IAE (Morishima *et al*, 2002), leading to the speculation that vascular obstruction due to intravascular thrombi might also be involved in the development of IAE.

Although several hypotheses on the pathological mechanism(s) of IAE have been reported, none have been verified experimentally, and to date, there are no animal models of IAE. The present thesis comprises two chapters. Chapter 1 describes the establishment of a murine model of IAE induced by lipopolysaccharide (LPS) treatment of IAV-infected neonatal mice. Results using this model show that pulmonary infection with IAV causes deterioration of LPS-induced encephalopathy and enhances the production of plasma inflammatory cytokines in neonatal mice. The pathology of these mice was similar to that of IAE patients with respect to histological changes in the CNS and the absence of direct

3

infection of the brain by IAV. The dynamics of plasma inflammatory cytokines were also similar to patients with IAE. Chapter 2 presents evidence of the potential role of apoptosis in the brain of the murine model of IAE established in Chapter 1. Increased apoptosis in the CNS is consistent with the previous reports of IAE patients (Morishima *et al*, 2002; Nakai *et al*, 2003; Nunoi *et al*, 2005); therefore, the murine IAE-like encephalopathy appears to share the same pathological mechanism with human IAE in terms of the increased permeability of the BBB. These results suggest that encephalopathy induced in neonatal mice treated with IAV and LPS is an appropriate animal model of IAE. Importantly, results using this model system indicate that LPS-induced hypercytokinemia and/or the involvement of endotoxemia in IAV infection are possible causes of IAE.

Chapter 1

Combined treatment with IAV and LPS induces an IAE-like encephalopathy in neonatal mice

Introduction

To date, there have been several reported animal models of IAE. In one widely-recognized model, mini-plasmin, a hemagglutinin processing protease, accumulates in the cerebral capillaries of mice with abnormal mitochondrial β-oxidation after non-neurotropic IAV infection (Yao *et al*, 2004). The accumulation of mini-plasmin allows non-neurotropic IAV to infect cerebral vascular endothelial cells, which triggers increased permeability of the BBB. However, IAV is not typically detected in the CNS of IAE patients, and therefore this model is not fully consistent with human IAE. Moreover, the mini-plasmin model is accompanied by fatty liver, similar to Reye's syndrome (Okita *et al*, 1996). But fatty liver is not associated with human IAE. Reye's syndrome is a well-known encephalopathy associated with influenza epidemics. The syndrome is closely linked to the administration of aspirin (Starko *et al*, 1980; Waldman *et al*, 1982). IAE is generally recognized as a disease entity that is distinct from Reye's syndrome. The time interval between onset of fever and the development of encephalopathy is much shorter in IAE than Reye's syndrome, the latter of which

is usually associated with an incubation time of several days or a few weeks. In addition, elevated serum hepatic enzyme and fatty degeneration of the liver are characteristics of Reye's syndrome (Starko *et al*, 1980). Thus, the murine model reported by Yao *et al* is, in effect, a model of Reye's syndrome, not IAE. In our laboratory, the effect of high fever on the development of IAE has been examined by intraventricular administration of prostaglandin E2 to neonatal mice infected with IAV. The significance of COX-2 in the development of IAE has been also examined using *COX-2* knockout mice. The results of these experiments have shown that neither high fever nor deletion of *COX-2* induces IAE in IAV-infected neonatal mice (not yet published data).

Sepsis is a condition characterized by uncontrolled bacterial infection, which induces severe systemic inflammatory response to microorganisms or their toxin. It affects many organs, including lungs, kidneys, heart, and CNS, with a high mortality rate. Septic encephalopathy is a common complication of sepsis, characterized by diffuse or multifocal neural dysfunction as a result of an inflammatory response with or without direct bacterial invasion of the brain (Papadopoulos *et al*, 2000). Administration of LPS, a structural component of the outer membrane of Gram-negative bacteria, induces pathological changes that mimic the process of sepsis (Alexander *et al*, 2008; Papadopoulos *et al*, 2000). The predominant microscopic changes associated with LPS-induced encephalopathy are vasogenic cerebral edema and neuronal damage (Bogdanski *et al*, 2000; Stolp *et al*, 2005). Although the mechanism of septic encephalopathy is

not fully elucidated, TNF-α has been implicated as a factor in the pathogenicity (Alexander *et al*, 2008). Septic encephalopathy is similar to IAE in terms of the involvement of inflammatory cytokines as well as CNS histopathology. Therefore, whether LPS-induced pathogenicity contributes to the development of an IAE was investigated.

Here, demonstrate that pulmonary infection with IAV enhanced the neuropathogenicity of LPS and induced encephalopathy with similar characteristics to human IAE, including CNS lesions, increased BBB permeability, inductions of inflammatory cytokines in the blood, and the absence of the brain by IAV.

Materials and Methods

Virus

Influenza A virus strain A/Aichi/2/68 (H3N2) was obtained from the Laboratory of Microbiology, Graduate School of Veterinary Medicine, Hokkaido University, and was propagated in the allantoic cavities of 10-day-old embryonated chicken eggs at 35°C for 48 h (Isoda *et al*, 2006). Virus-containing allantoic fluid was collected, stored at -70°C, and used as the viral stock.

Mice

Pregnant ICR mice were purchased from Charles River Laboratories Japan,

Inc. (Kanagawa, Japan). Seven-day-old suckling mice were treated as described in the following section. To minimize variability associated with the use of different maternal mice, the number of neonatal mice was maintained at around 12 per female mouse. All animal studies were carried out with the approval of the Laboratory Animal Experimentation Committee, Graduate School of Veterinary Medicine, Hokkaido University, and were consistent with the international standards of the Association for Assessment and Accreditation of Laboratory Animal Care. All viral infections were carried out in the P3 biosafety compartment of the Graduate School of Veterinary Medicine, Hokkaido University.

Inoculation of mice with IAV and LPS

Seven-day-old mice were anesthetized by isoflurane inhalation and inoculated through both nostrils with 10 μl (1×10^5 PFU) of IAV. The mice were subsequently inoculated twice with LPS from *E. coli* O55:B5 (Sigma, St. Louis, MO), as follows: briefly, mice received an inoculation of 0.5 μg/g LPS into hind limb muscle 3 days post infection (dpi), followed by a second inoculation of 20 μg/g LPS into the peritoneal cavity 24 h after the first LPS inoculation (Fig. 1). Control mice received a similar schedule of equivalent volumes of sterile saline without IAV or LPS. Mice were monitored until 7 dpi, or were subjected to whole blood collection under anesthesia followed by necropsy, between 4-7 dpi at 6, 12 or 24 h intervals, as indicated.

Histopathological analysis and semiquantitative evaluation of microscopic changes

At necropsy, tissue samples from the liver, spleen, kidneys, heart, lungs, thymus and brain were collected from mice, fixed in 20% neutral buffered formalin solution, and then embedded in paraffin wax. Tissue samples were cut into 4 μm thick sections and stained with hematoxylin-eosin in preparation for light microscopy. Histopathological changes in the thymus, lungs and brain were semi-quantitatively scored from 0 (absent) to 3 (severe) on the basis of the distribution and severity of the lesions. Sections were prepared from predetermined areas of the thymus, lungs and brain. For the evaluation of pulmonary lesions, 2 sections from the left lung and 2 sections from the anterior and caudal lobes of the right lung (4 total) were obtained. For the evaluation of brain lesions, sections from the frontal lobe, diencephalon, occipital lobe, brain stem, and medulla oblongata (5 total) were obtained. The criteria for scoring each organ were as follow: 0, no significant lesions; 1, localized and very mild lesions; 2, moderate lesions distributed on more than half of the sections; 3, moderate-to-severe lesions distributed diffusely over almost all of the sections.

Immunohistochemistry (IHC)

Serial sections were stained with a streptavidin-biotin immunoperoxidase complex using a Histofine SAB-PO kit (Nichirei Corp., Tokyo, Japan). To restore antigens, the sections were treated with 0.01 M phosphate buffered saline (PBS)

containing 0.1% trypsin (Becton Dickinson, Mountain View, CA, USA) for 20 minutes (min) at 37°C. Diluted hyperimmune serum of the rabbit immunized with inactivated influenza A virus (A/Whistling swan/Shimane/499/83) (1:5000; produced in our laboratory) was applied to the sections for approximately 12 h at 4°C (Matsuda *et al*, 2004). The chromogenic reaction was carried out by incubating the sections in a solution of 0.05 M Tris-HCl buffer (pH 7.6) containing 0.02% 3, 3'-diaminobenzidinetetrahydrochloride (DAB; Dojindo Laboratories, Kumamoto, Japan), 0.005% H_2O_2, and 0.01 M imidazole (Sigma). The sections were counterstained with Mayer's hematoxylin. As a negative control, the primary antibody (hyperimmune serum) was replaced with 0.01 M PBS.

Evaluation of BBB integrity

The integrity of the BBB was evaluated by Evans Blue (EB; Kanto Chemical Corp., Tokyo, Japan) extravasation, as described previously (Bigdeli and Khoshbaten, 2008; Fukui *et al*, 2003). Briefly, mice were injected intraperitoneally with 50 μl of a filtered solution of 2% EB in sterile saline. The mice were anesthetized 2 h after EB injection and the brains were rapidly removed. After gross inspection, pieces of the brain were collected to quantify the deposited EB. EB dye in the brain was extracted with 500 μl of formamide for 24 h at 38°C. The amount of EB in supernatants was measured against a standard of 90% formamide in saline at 630 nm using a plate reader (Multiscan Ascent, Thermo Labsystems,

Franklin, MA, USA) and EB levels were calculated in units of ng/g of brain tissue using a standard curve.

Determination of plasma cytokine concentrations

Whole blood was collected into blood collection tubes containing EDTA (Terumo Medical Corp., Elkton, MD, USA). Plasma was obtained by centrifugation of whole blood at 3,500 G for 2 min and then frozen at -70°C until use. Plasma cytokine levels were determined using a mouse inflammation cytometric bead array kit and a FACSArray[TM] bioanalyzer (Becton Dickinson, Mountain View, CA, USA) (Li *et al*, 2007; Morgan *et al*, 2004), according to the manufacturer's instructions. Standard curves were determined for each cytokine in the range of 20-5,000 pg/ml. The following cytokines were measured: IL-6, IL-10, monocyte chemotactic protein (MCP)-1, interferon (IFN)-γ, TNF-α, and IL-12p70.

Plaque assay

Plaque assays were performed to evaluate virus titers in lungs and brain, as previously described (Tsuda *et al*, 2009). Briefly, Mardin-Darby canine kidney (MDCK) cells were grown in Eagle's minimal essential medium (EMEM; Nissui Pharmaceutical Co., Tokyo, Japan) supplemented with 10% inactivated fetal bovine serum and 2 mM L-glutamine. Pieces of mouse tissue were homogenized in EMEM at 4°C to make 10% tissue homogenate. Confluent monolayer of MDCK cells were inoculated with 10-fold dilutions of homogenized sample and then

11

incubated for 1 h at 37°C. Diluted homogenate was removed, and then the cells were washed with PBS and overlaid with EMEM containing 1% BactoAgar (Becton Dickinson) and 0.0005% acetyl trypsin. Cells were incubated for 48 h at 37°C, followed by staining with 0.005% neutral red for 12 h.

Results

General status and survival rates of experimental animals

Influenza A virus, LPS, or both (IAV+LPS) were inoculated into 1 week-old ICR mice. Mice in the IAV group exhibited signs of depression, rough fur, and emaciation at 3-4 dpi, which progressively worsened with time. Mice in the LPS and IAV+LPS groups exhibited the same symptoms, as well as diarrhea and a sluggish response to manual stimulation within several hours of LPS inoculation. The general symptoms appeared more severe in the IAV+LPS group as compared to the IAV or LPS groups. All of the mice survived in the LPS group survived, whereas 93% and 68% of mice in the IAV and IAV+LPS groups survived, respectively (Fig. 2).

Histopathological changes

Histopathology revealed evidence of multifocal bronchointerstitial pneumonia in the lungs of mice in the IAV and IAV+LPS groups. In the IAV group, the lesions were mainly located around the bronchioles and sometimes involved

12

peripheral alveoli (Fig. 3). The bronchiolar and alveolar walls were thickened by infiltration of mononuclear cells and neutrophils. Bronchiolar lumina and alveoli also contained a small number of sloughed epithelial cells (Fig. 4). The lungs of mice from the IAV+LPS group showed microscopic pulmonary lesions that were similar in quality, distribution and severity to the IAV group (Fig. 5).

Multifocal microbleeding, irregular dilation of perivascular spaces, and neutrophilic infiltration were evident in the brains of mice in the LPS and IAV+LPS groups (Figs. 6 and 7). The lesions were usually located in the cerebral cortex and brain stem. Infiltrated neutrophils had a mildly sponge-like appearance and astrocytes were degenerated in some areas (Fig. 8), especially the peripheries of areas of neutrophil–infiltration and scattered microhemorrhage. Degenerated astrocytes had round, swollen, and vacuolated nuclei (Fig. 8). These microscopic changes were acute and transient; they appeared 24 h after the second LPS inoculation, became more pronounced up to 48 h, and then subsided at 72 h. There were no significant lesions in the brains of the IAV group throughout the course of the experiment. Histopathological changes of the brain in the IAV+LPS group were more prominent than the LPS group. Marked changes were absent in all other organs, with the exception of a depletion of thymic lymphocytes.

Semi-quantitative histopathological analysis revealed no significant differences in scores for thymic lymphocytic depletion and bronchointerstitial pneumonia between the IAV and IAV+LPS groups. Cerebral histopathological

changes in the IAV+LPS group were more severe than those of the LPS group, in particular, cerebral microbleeding (Table 1).

Cerebrovascular permeability

To evaluate cerebrovascular permeability, EB dye was injected to the abdominal cavity of mice, and then the concentrations of dye in the brains of IAV, LPS, and IAV+LPS groups were compared. Overall, the color of the brains of mice in the IAV group was normal (Fig. 9A). However, the brains of the LPS and IAV+LPS groups had a noticeably bluish tinge. The brains of IAV+LPS mice appeared to be more severely tinted than those of the LPS group (Fig. 9A).

To quantify these apparent differences in EB dye concentration, dye density in the brains of the LPS and IAV+LPS groups was measured by absorption spectrometry. The brains of mice in the IAV+LPS group contained significantly higher levels of dye than the LPS group ($P < 0.05$; Fig. 9B). These results suggested that the integrity of the BBB was significantly deteriorated in the IAV+LPS group. This was consistent with the results of semi-quantitative histopathological analysis (Table 1), in which the IAV+LPS group exhibited more severe cerebral lesions than the other groups.

The induction of cytokines in plasma

To determine whether IAV infection affected the induction of inflammatory cytokines by LPS as well as the severity of encephalopathy, plasma

14

cytokine concentrations were measured. Cytokine levels in the plasma of each group were measured 6, 12, and 24 h after the LPS inoculations. In the LPS and IAV+LPS groups, the induction of most inflammatory cytokines was upregulated 6 h after LPS inoculation (Fig. 10). The serum concentrations of TNF-α and IL-6 in the IAV+LPS group were significantly higher than those in the IAV and LPS groups (Fig. 10A and C). In addition, the concentrations of MCP-1 and IL-10 in the IAV+LPS group were significantly higher than in the IAV group (Fig. 10B and D). In contrast, the level of IFN-γ in the IAV group tended to be higher than the other groups, but this difference was not statistically significant (Fig. 10E). Elevated cytokine levels in the LPS and IAV+LPS groups returned to normal or lower than normal levels 24 h after LPS stimulation. The serum concentration of IL-12p70 was unchanged in all groups at all time points.

Distribution of viral antigens and viral titers

The presence of viral antigen in the lungs of the IAV and IAV+LPS groups was analyzed by IHC (Figs. 11 and 12). Many IAV antigen-positive cells were distributed in a multifocal manner along the bronchiolar walls of mice in both groups. Positive nuclear and occasionally cytoplasmic staining of bronchiolar epithelial cells was observed. In addition, some alveolar epithelial cells were positive for IAV antigen. These cells exhibited a multifocal distribution pattern in alveolar walls thickened by inflammatory responses. There were no obvious differences in the localization and number of antigen positive cells between the

15

IAV and IAV+LPS groups. The lungs from the LPS group were entirely negative. Other organs, including liver, spleen, kidneys, heart and brain (Fig. 13), were negative for IAV antigen in all mice from all groups.

Viral titers in the lungs of the IAV and IAV+LPS groups at 5 dpi were 6.62±0.08 and 6.42±0.13 $\log_{10}$PFU/g (means ± SEM), respectively. There was no statistical difference between the two groups (Student's *t*-test). Plaque assays failed to detect IAV in the brains of the IAV and IAV+LPS groups.
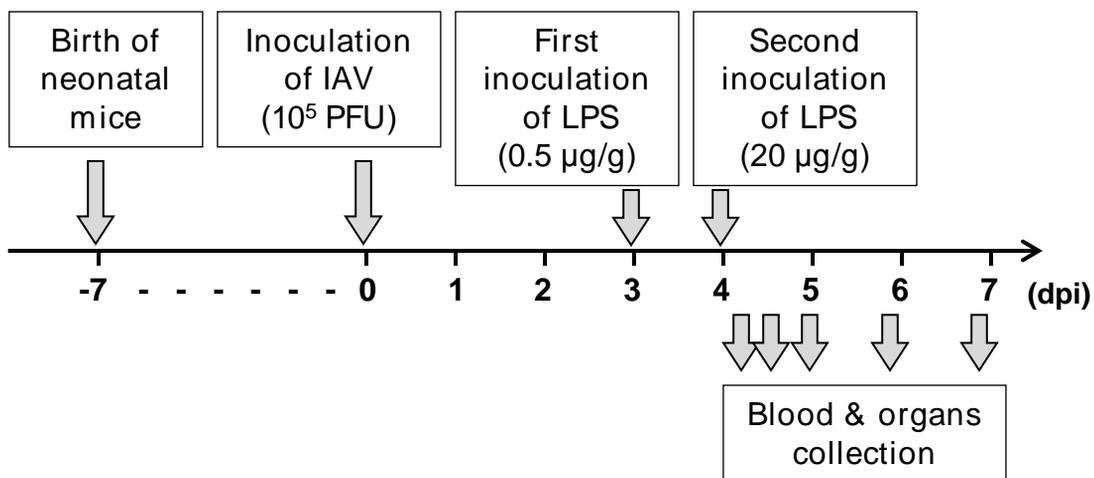
Fig. 1. Time schedule of inoculation with IAV and LPS. Seven day-old mice are infected with IAV at 0 dpi, and then inoculated with LPS at 3 and 4 dpi. The mice are submitted to sample collection at 6, 12, 24, 48 and 72 h after the 2nd LPS inoculation.
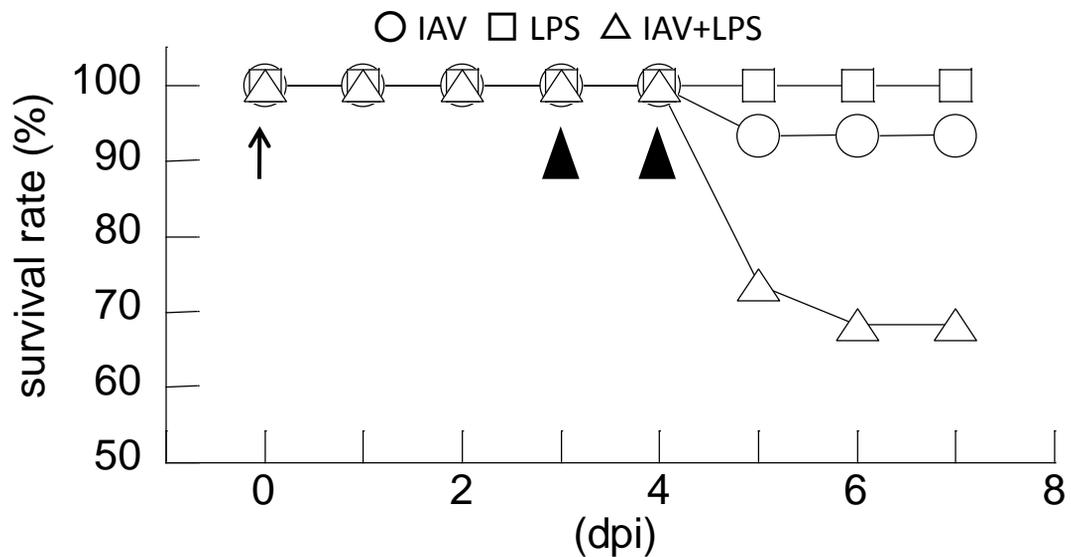
Fig. 2. Survival rates of the IAV, LPS and IAV+LPS groups. The mice of the IAV and LPS groups show 96% and 100% of survival rates, respectively. However The mice of the IAV+LPS group shows 68% of survival rate, relatively low than the others. The arrow shows intranasal inoculation with IAV (IAV and IAV+LPS groups) or saline (LPS group). The arrowheads show inoculations of LPS (LPS and IAV+LPS groups) or saline (IAV group) at 3 and 4 dpi.

Fig. 3.   Lung, mouse, the IAV group, 6 dpi. Focal bronchointerstitial pneumonia due to IAV infection. Moderate inflammation is mainly distributed around the bronchi (asterisks) and expands to the peripheral alveoli. Bar = 500 μm. Hematoxylin-eosin stain.

Fig. 4.   Lung, mouse, the IAV group, 6 dpi. Higher magnification of the bronchointerstitial pneumonia indicated in Fig. 3. Alveolar walls are thickened by infiltration of inflammatory cells and proliferation of alveolar epithelial cells. Some of alveoli contain small number of floated epithelial cells and alveolar macrophages (arrows). Bar = 100 μm. Hematoxylin-eosin stain.

Fig. 5.   Lung, mouse, the IAV+LPS group, 6 dpi. Bronchointerstitial pneumonia almost same as that observed in the IAV group (Fig. 3, 4). Alveolar walls are thickened by infiltration of mononuclear leukocytes. Bar = 100 μm. Hematoxylin-eosin stain.
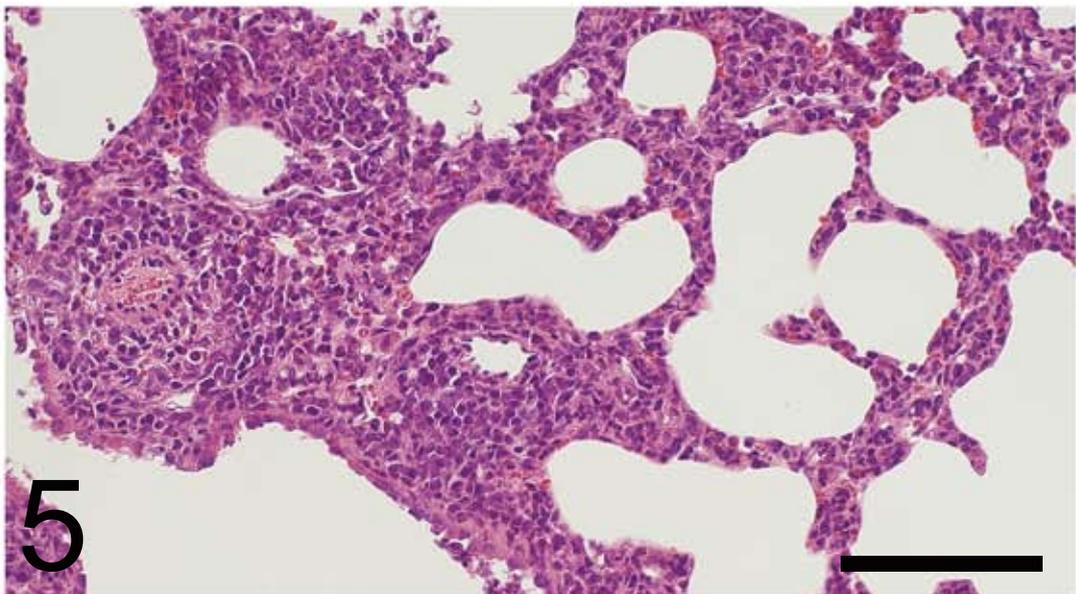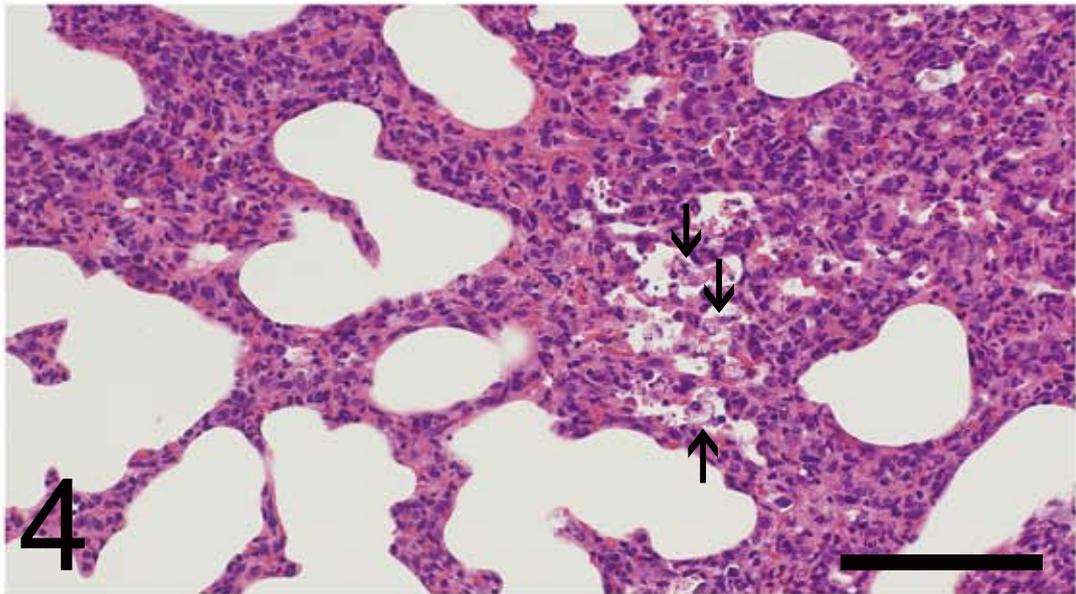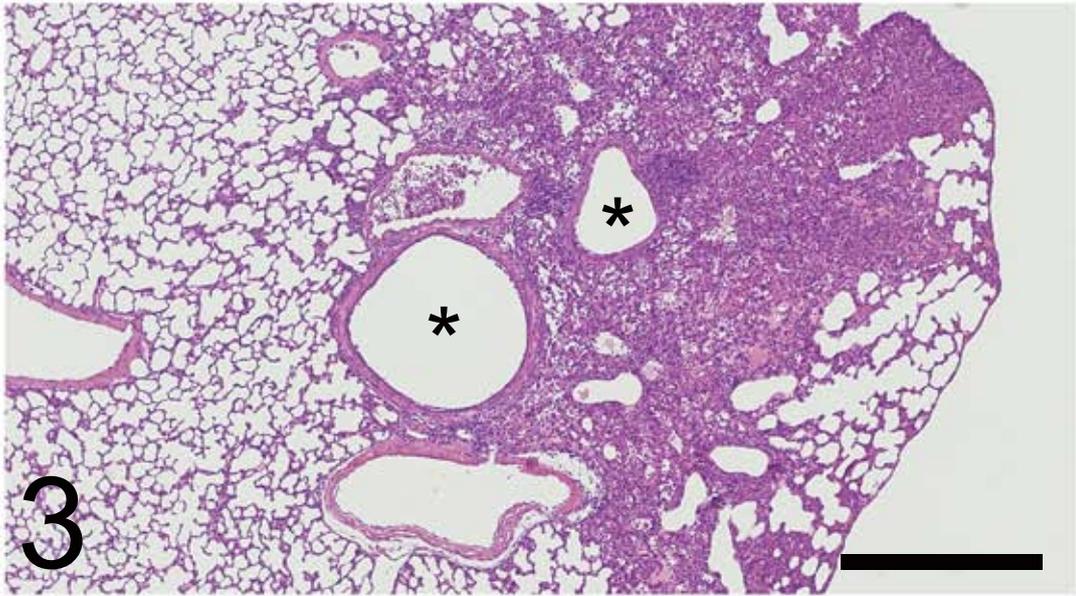
Fig. 6. Brain, mouse, the LPS group, 48 h after the LPS inoculations. Some perivascular spaces dilate irregularly (arrowheads). Neutrophils infiltrate in the parenchyma (arrows). Bar = 50 μm. Hematoxylin-eosin stain.

Fig. 7. Brain, mouse, the IAV+LPS group, 48 h after the LPS inoculations. There are irregular dilation of some perivascular spaces (filled arrowheads) and infiltration of neutrophils (arrows). In addition, microbleeding (open arrowhead) is conspicuous. The inset demonstrates hyaline droplet formations in a dilated perivascular space. Bar = 50 μm. Hematoxylin-eosin stain.

Fig. 8. Bain, mouse, the IAV+LPS group, 48 h after the LPS inoculations. The neuropils on the right half of the photograph show mild spongy appearances. Some nuclei of astrocytes are swelled and show vacuolated appearances (arrows). Bar = 50 μm. Hematoxylin-eosin stain.
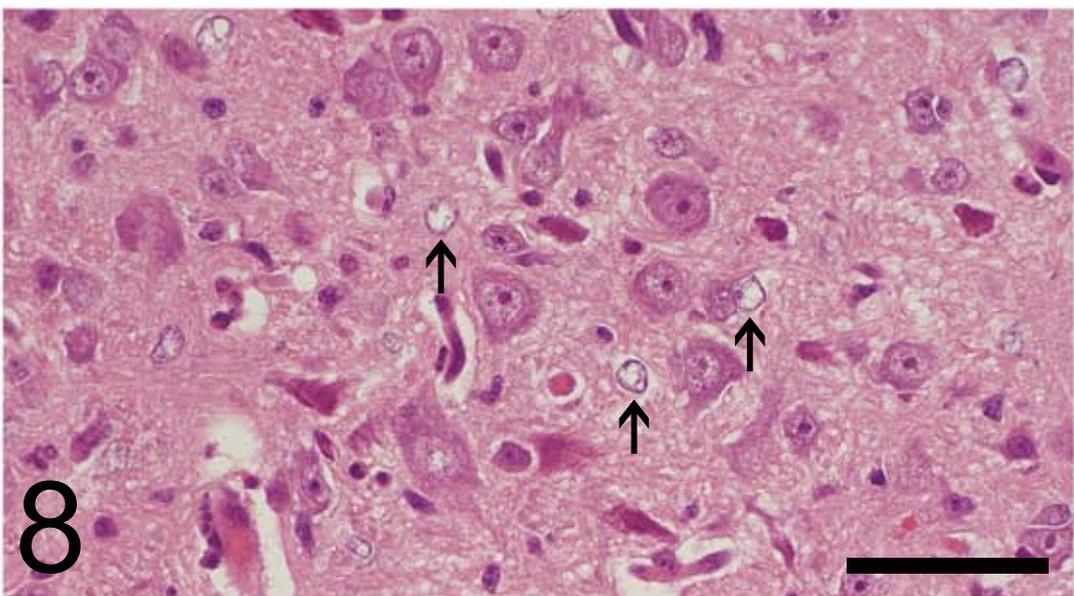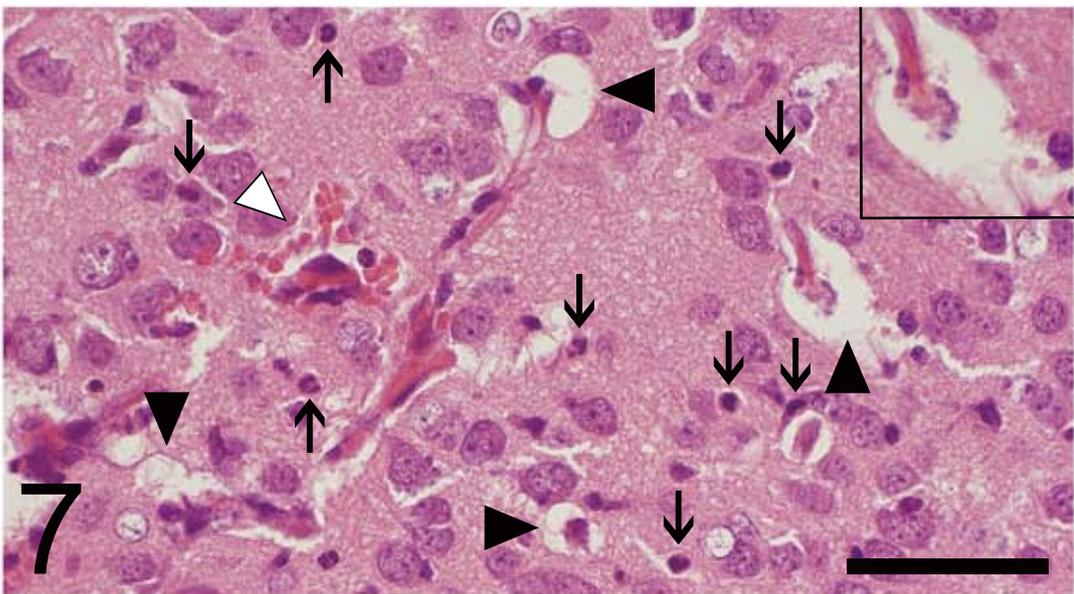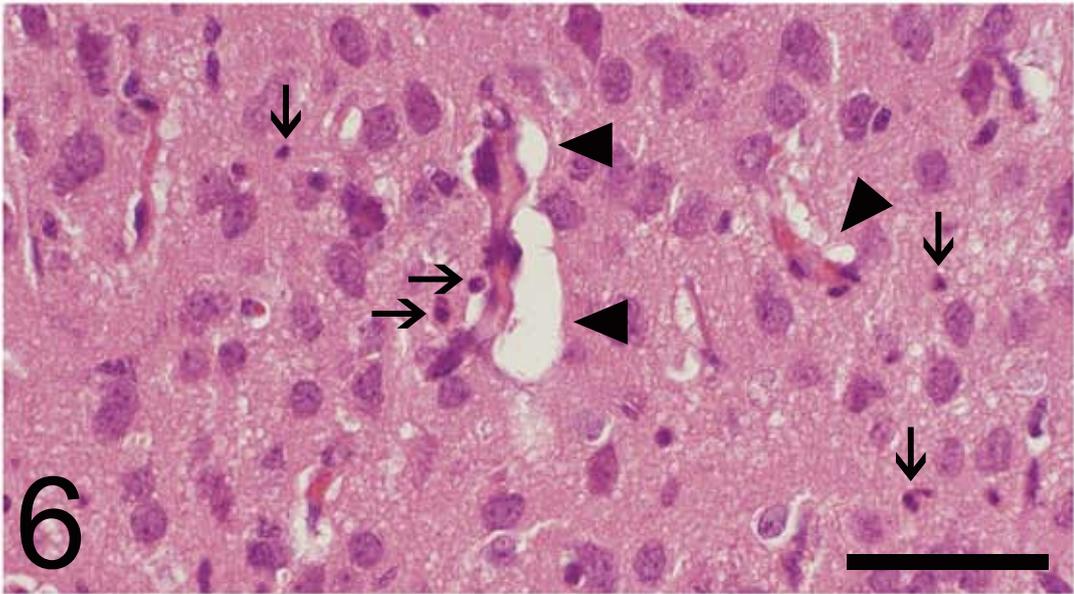
Table 1   Semiquantitative analysis of microscopic changes.

Groups	Time after the LPS inoculation	Thymus Lymphocytic depletion	Lungs Interstitial pneumonia	Brain Microhemorrhage	Brain Neutrophilic infiltration	Brain Edema
IAV		0 (0-0)[a]	2 (2-2)	0 (0-0)	0 (0-0)	0 (0-0)
LPS	48 hrs	2 (1.25-2)	0 (0-0)	1.5 (1-2)	2.5 (1.25-3)	2 (1.25-2)
	72 hrs	2 (2-2)	0 (0-0)	0 (0-0)	2 (1.5-2)	2 (0.5-2)
IAV+LPS	48 hrs	3 (3-3)	1.5 (1-2)	3 (3-3)*	3 (3-3)	2 (2-3)
	72 hrs	2 (1.5-2)	2 (2-2)	0 (0-0)	2 (1.5-2)	1 (1-1.5)

[a] Semiquantitative scores of microscopic changes are represented as mean median of values (25-75 percentile) in this order. 0: no obvious change, 1: focal mild change, 2: multifocal moderate change, 3: diffuse severe change. The microhemorrhage, neutrophilic infiltration and edema in brain tend to be more prominent in the IAV+LPS group than the LPS group. There is no obvious difference in the scores of interstitial pneumonia between the IAV and IAV+LPS groups. * $P < 0.05$. Statistical differences were analyzed using Mann-Whitney U test.
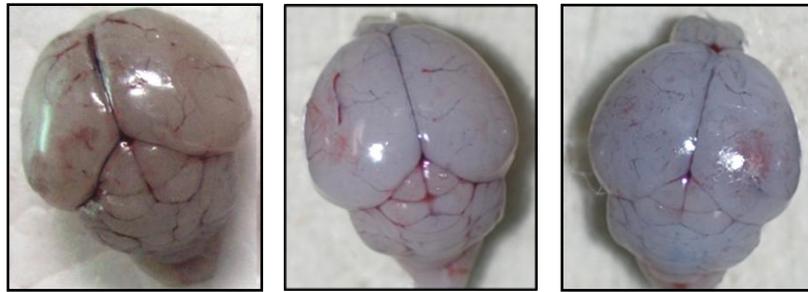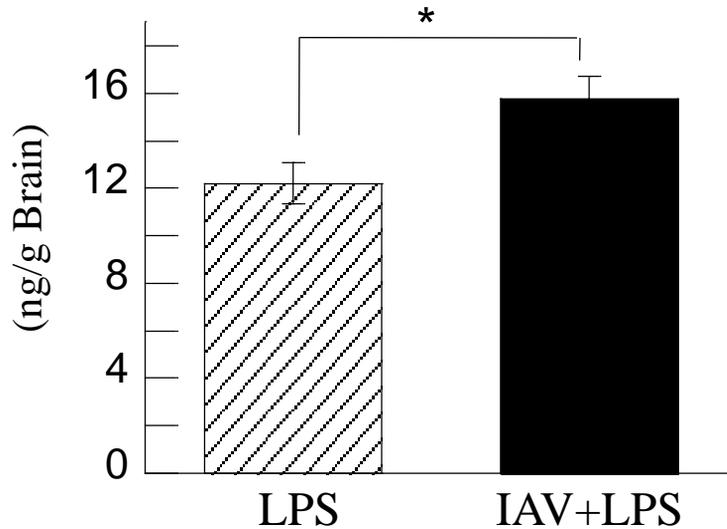
Fig. 9. Estimation of the BBB integrity. (A) Representative photographs of the brain from the IAV, LPS and IAV+LPS group mice injected intraperitoneally with EB dye. The brains were collected 48 h after LPS inoculations. The brain from the IAV group appears to be normal. Those from the LPS and IAV+LPS groups are stained blue, and the latter is more deeply stained than the former. (B) Quantification of EB dye extracted from the brains. The IAV+LPS group shows significantly higher value than LPS groups. Each error bar means standard error. The statistical comparison was performed using Student's *t*-test (* $P < 0.05$).
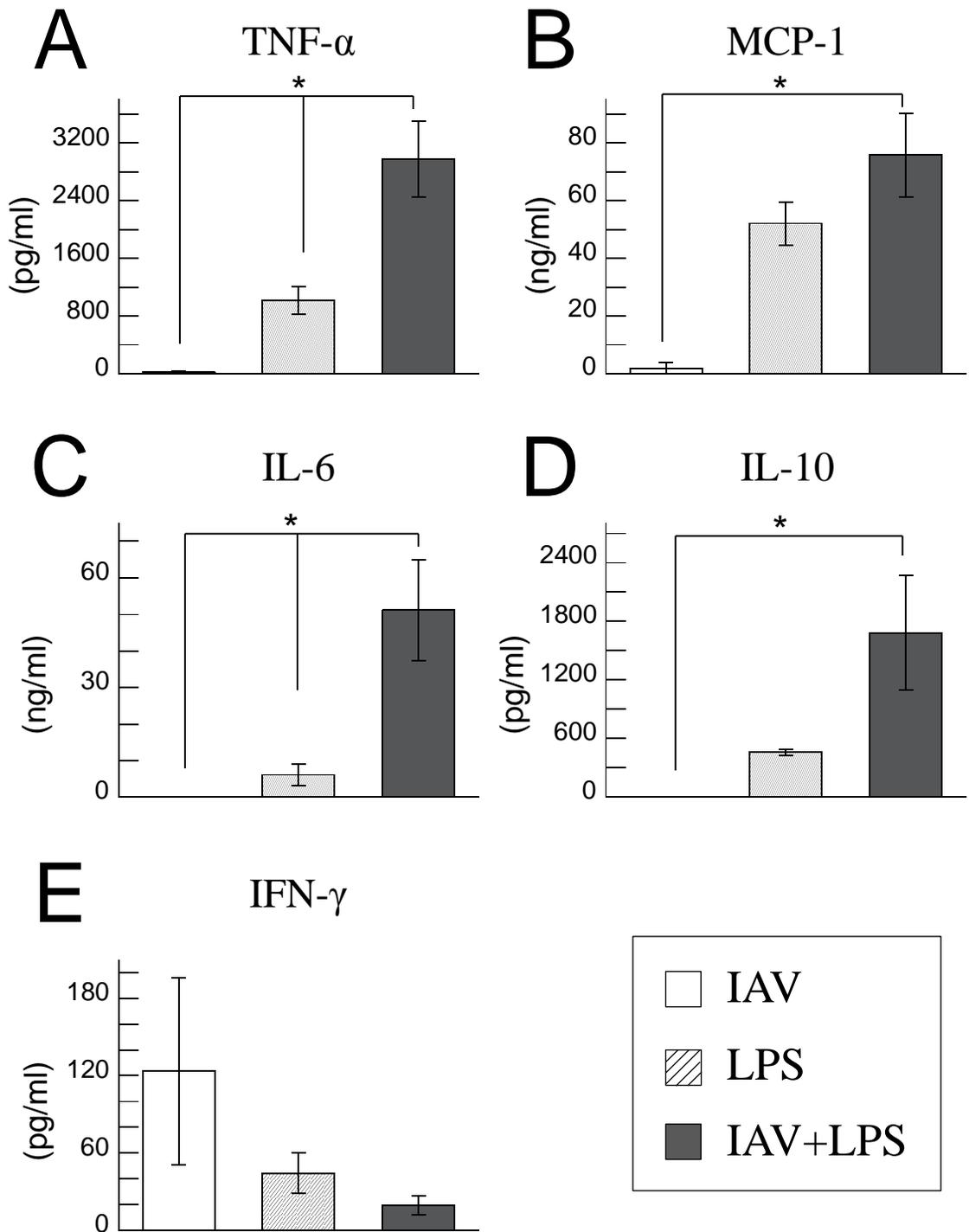
**Fig. 10.** Quantitative analysis of the productions of TNF-α (A), MCP-1 (B), IL-6 (C), IL-10 (D), IFN-γ (E) in plasma. Plasma was collected from the IAV (open column), LPS (striped column), and IAV+LPS (filled column) groups at 6 h after the 2nd LPS (or saline) inoculation. Each error bar means standard error. Differences among means were statistically analyzed using Tukey-Kramer multiple comparison tests (* $P < 0.01$).

Fig. 11.   Lung, mouse, the IAV group, 6 dpi. Some nuclei of bronchiolar and alveolar epithelial cells (allows) show positive reaction for IAV antigens. Asterisks indicate bronchiolar space. Bar = 50 μm. IHC (IAV antigens) by the streptavidin-biotin immunoperoxidase complex method, Mayer's hematoxylin conterstain.

Fig. 12.   Lung, mouse, the IAV+LPS group, 6 dpi. Some nuclei of bronchiolar and alveolar epithelial cells (allows) show positive reaction for IAV antigens. The asterisk indicates bronchiolar space. There are no difference on the distribution and frequency of IAV antigens-positive cells between the IAV and IAV+LPS groups. Bar = 50 μm. IHC (IAV antigens) by the streptavidin-biotin immunoperoxidase complex method, Mayer's hematoxylin conterstain.

Fig. 13.   Brain, mouse, the IAV+LPS group, 6 dpi. Brains are entirely negative for IAV antigens. Bar = 50 μm. IHC (IAV antigens) by the streptavidin-biotin immune-peroxidase complex method, Mayer's hematoxylin conterstain.
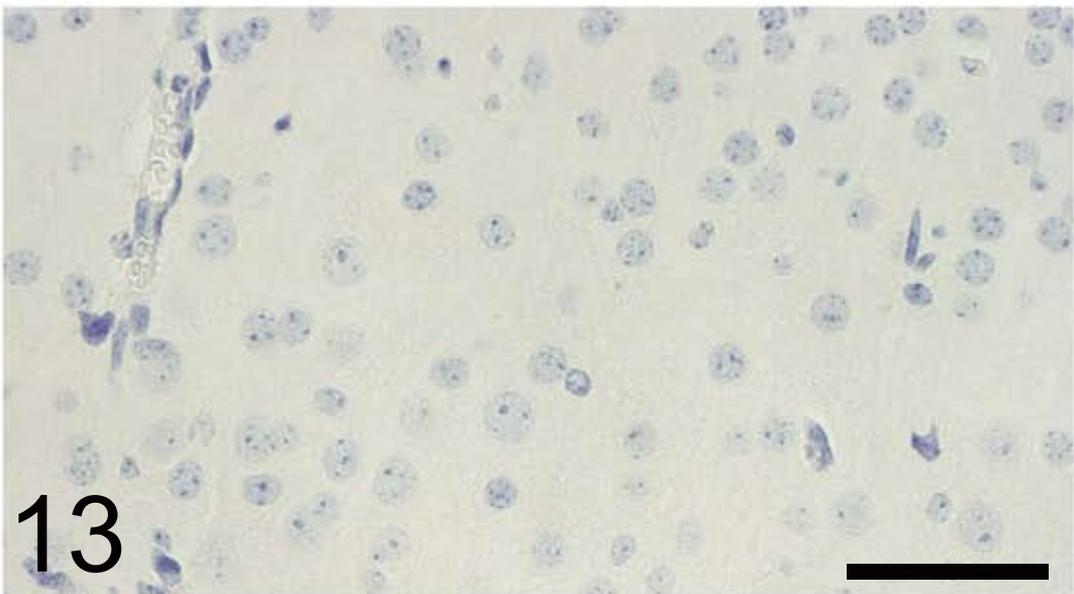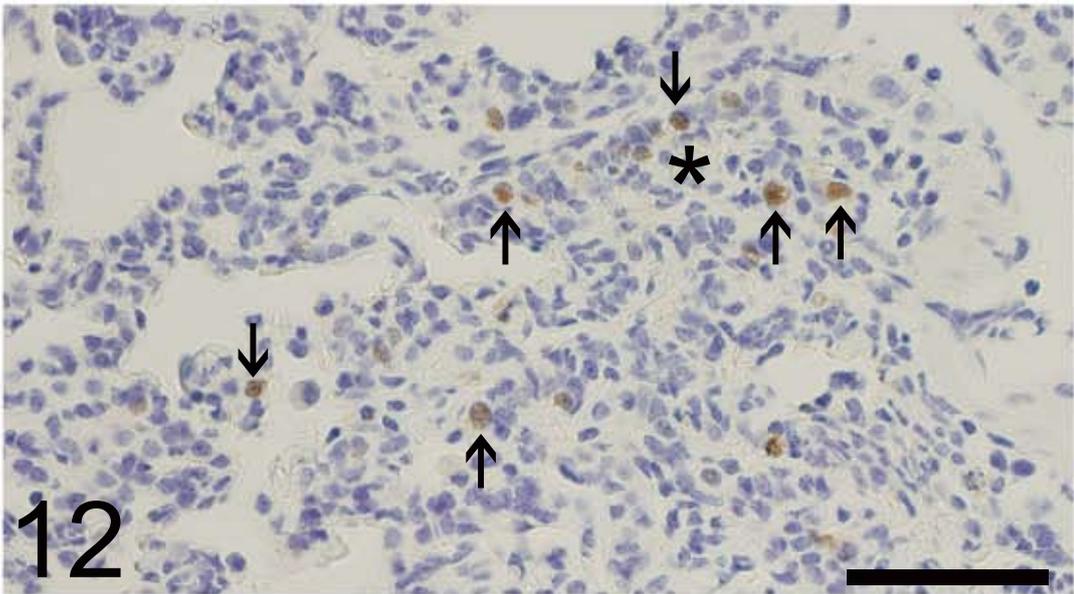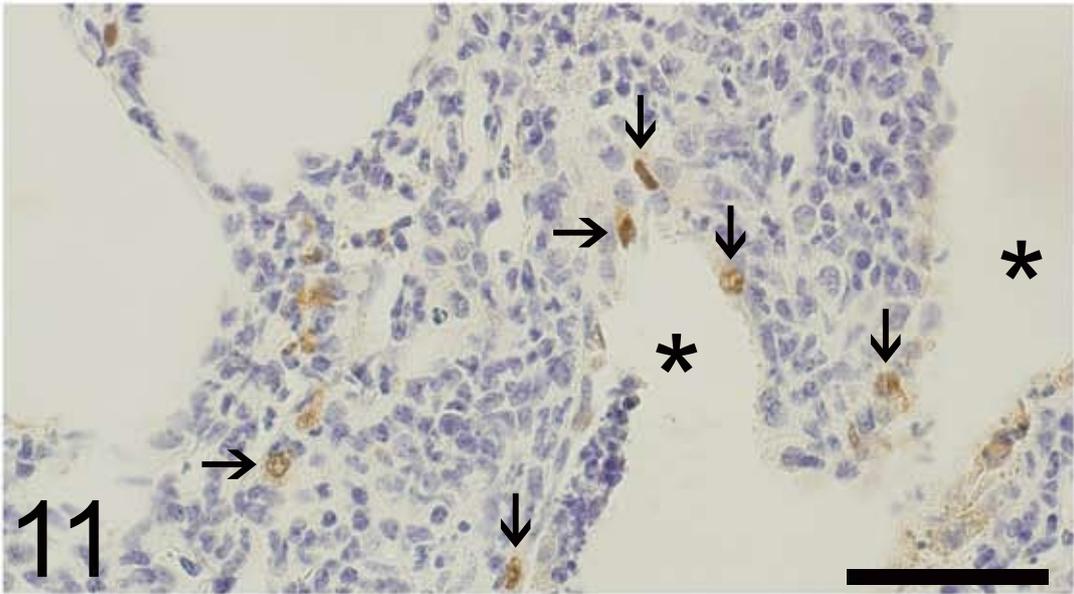
Discussion

Early diagnosis, prevention and therapy of IAE have yet to be established, primarily because the pathological mechanism of the disease is unknown. In this study, neonatal ICR mice were submitted to the infection experiment, because IAE most frequently occurs in children aged 2-4 years. Young children and neonatal animals are believed to have an immature BBB (Banks, 2009; Urayama *et al*, 2004). Here, an H3N2 subtype of IAV (A/Aichi/2/68) was used as the viral source because this subtype of virus is most commonly recovered from IAE patients.

A subset of neonatal mice infected with IAV also received LPS inoculations. Survival rates of the IAV, LPS, and IAV+LPS groups were 96%, 100% and 68%, which suggested that the pathological condition induced by IAV+ LPS treatment was more severe than that induced by either agent alone. Histopathologically, H3N2 IAV infection of neonatal mice induced moderate bronchointerstitial pneumonia. There were no differences in the severity of the pneumonia, localization of viral antigens, and viral titers in lungs between IAV and IAV+LPS mice. Histopathological analysis revealed microhemorrhage and irregular dilation of perivascular spaces in the brains of the LPS and IAV+LPS groups. These results were consistent with previous reports of LPS-induced encephalopathy (Bogdanski *et al*, 2000; Stolp *et al*, 2005). In addition, these microscopic lesions in the brain suggested the occurrence of cerebral vascular damage in the LPS and IAV+LPS groups. Mild neutrophilic infiltration was likely

28

to be a secondary reaction to the brain damage. Swelling of astrocytes was non-specific change commonly observed in many types of CNS disorders (Hirano, 1991). Histological changes in the CNS were more severe in the IAV+LPS group than the LPS group. The histopathological and IHC findings suggested that IAV infection aggravates LPS-induced encephalopathy; conversely, LPS inoculation did not appear to affect the respiratory complications of IAV infection. Therefore, it was hypothesized that deterioration of CNS damage is a direct cause of the increased mortality of mice in the IAV+LPS group.

The pathological mechanism of LPS-induced encephalopathy remains to be elucidated, but previous studies have suggested the involvement of multiple factors, including inflammatory cells and their mediators, reduced cerebral blood flow, and disruption of the BBB (Papadopoulos *et al*, 2000). In the current study, there was no evidence of intravascular thrombi in any mice. Thus, it is unlikely that microvascular infarction was the cause of the cerebral and/or cerebrovascular damage in the LPS and IAV+LPS groups. Previous *in vitro* studies using human peripheral blood leukocytes have shown that the production of TNF-α, IL-1, and IL-6 is enhanced by combined treatment with IAV and LPS (Lundemose *et al*, 1993; Nain *et al*, 1990). Similarly, infection of infant ferrets with IAV enhances their susceptibility to the lethal effects of endotoxin (Jakeman *et al*, 1991). In the current study, pulmonary infection with IAV enhanced the production of TNF-α and IL-6 induced by LPS in the plasma of the IAV+LPS group, in line with these previous reports. The concentrations of MCP-1 and IL-10 were higher in the blood

of the IAV+LPS group than the IAV group, although there were no statistical differences between the LPS and IAV+LPS groups. There were no statistical differences in plasma IFN-γbetween any groups. The mechanism of enhanced cytokine production following IAV and LPS treatment was not revealed by the current results. However, other studies have suggested that IAV and LPS concurrently activate several common transcription factors responsible for cytokine gene expression, including NF-κB, IRF, and AP-1 (Julkunen *et al*, 2000; Kawai and Akira, 2006). In addition, LPS is thought to potentiate cytokine synthesis at the post-transcriptional level (Han *et al*, 1990; Nain *et al*, 1990). In the current study, the levels of plasma cytokines correlated positively with the severity of brain lesions. The levels of plasma cytokines peaked at about 6 h after LPS inoculation, which was earlier than the appearance of cerebral lesions 24 h after LPS inoculation. Thus, it is possible that the over-induction of inflammatory cytokines contributed to the enhancement of LPS-induced encephalopathy in mice infected with IAV. In particular, the elevated concentrations of TNF-α and IL-6 may contribute to cerebral vascular damage, as these cytokines play an important pathological role in LPS-induced encephalopathy (Alexander *et al*, 2008). The production of MCP-1 possibly associates with the neuropathogenicity induced by LPS (Kumai *et al*, 2004), as well as TNF-α and IL-6, although it was unclear whether MCP-1 contributed to the exacerbation of the CNS damage in the IAV+LPS group. IL-10 is one of anti-inflammatory cytokines, which effectively down-regulates the production of inflammatory cytokines, including TNF-α, IL-1,

30

IL-6, and IFN-γ (Mosser and Zhang, 2008; Stenvinkel *et al*, 2005). Secretion of IL-10 usually follows stimulations of LPS and TNF-α with a latency of a few hours (Stenvinkel *et al*, 2005). In this examination, the production of inflammatory cytokines was transient, since their concentrations already reduced to normal levels 24 h after the LPS inoculation. The induction of IL-10 might contribute to the subsequent reduction of cytokine production, although the relationship between increased IL-10 and the CNS damage was unclear.

The pathology of IAE is believed to involve vasogenic brain edema due to damage to vascular endothelial cells without invasion of IAV into the brain (Morishima *et al*, 2002). It has also been suggested that elevated cytokines such as TNF-α and IL-6 cause IAE (Aiba *et al*, 2001; Ichiyama *et al*, 2003; Ito *et al*, 1999; Toovey, 2008). In the current study, IAV+LPS mice exhibited an IAE-like encephalopathy, in respects of vasogenic brain lesions, dynamics of plasma inflammatory cytokines, and the absence of direct infection of the brain by IAV. These results indicate that LPS inoculation of IAV-infected neonatal mice represents an animal model of IAE, and that hypercytokinemia and/or the involvement of endotoxemia in IAV infection is a putative mechanism of IAE. Children sometimes have diarrhea with influenza, and the alteration of intestinal flora induced by diarrhea may cause endotoxemia. Chronic inflammation, including otitis media and tonsillitis is also common in children. When children with chronic gram-negative bacterial infection are infected by IAV, they may cause the similar condition to the murine model in the current study.

Summary

Influenza virus-associated encephalopathy (IAE) is a highly lethal neural complication of IAV infection that affects primarily children aged younger than 5 years. The brain pathology of IAE is characterized by peracute brain edema with evidence of an impaired BBB. The pathogenesis of IAE, however, remains unclear. Since the CNS pathology of IAE is similar to that of septic encephalopathy due to endotoxemia, here we examined the effect of combined treatment of 7 day-old neonatal ICR mice with IAV and LPS. Pulmonary infection with IAV enhanced the neuropathogenicity of LPS in neonatal mice. Mice that received combined treatment of IAV and LPS exhibited an encephalopathy that was similar to human IAE with regards to CNS histopathology and the absence of direct infection of the brain with IAV. Mice treated with IAV+LPS also exhibited increased BBB permeability and acute induction (within 6 h of LPS inoculation) of plasma inflammatory cytokines. The increased BBB permeability and hypercytokinemia observed in IAV+LPS mice were consistent with the hallmarks of IAE. Thus, we have developed a candidate murine model of IAE.

Chapter 2

Apoptosis of vascular endothelial cells and astrocytes as a possible cause of the brain lesion in a murine model of IAE

Introduction

Lipopolysaccharide (LPS) is a well-known inducer of various bioactivities. Following systemic LPS stimulation, recognition of LPS by host cells occurs through a series of receptor-mediated interactions (Akira *et al*, 2006; Beutler and Rietschel, 2003; Lu *et al*, 2008). LPS in the bloodstream binds to a shuttle protein, and then connects to CD14, a receptor protein expressed on the cell surface. LPS is then transferred to MD-2, which associates with the extracellular portion of Toll-like receptor (TLR) 4 (Akira *et al*, 2006). TLR4, a key molecule of LPS signaling, induces the activation of several transcription factors, such as NF-κB and AP-1 (Janssens *et al*, 2003; Kawai and Akira, 2006; Takeda and Akira, 2004), which results in the induction of expression of many immune factors, including inflammatory cytokines and chemokines. Previous reports have shown that TLR4 is expressed on a variety of somatic cells, including immunocompetent cells, vascular endothelial cells, and epithelial cells of the lungs, kidneys, and intestine (Lin *et al*, 2007; Takahashi *et al*, 2009; Zhou *et al*, 2009). Inflammatory cytokines that are activated by LPS stimulation, such as TNF-α, IL-1β, and IL-6, as well as

AP-1, can induce blood coagulation, vasoconstriction, inflammation, vulnerability of endothelial tight junctions (TJ), and apoptosis (Choi *et al*, 1998; Harkness *et al*, 2000; Merrill and Benveniste, 1996; Paul *et al*, 2003; Schulze *et al*, 1997; Vezzani *et al*, 2008; Wilson and Young, 2003).

In Chapter 1, it was demonstrated that infection of 7-day-old neonatal ICR mice with influenza A virus A (IAV) enhanced LPS-induced encephalopathy and the production of plasma inflammatory cytokines. Histopathologically, mice inoculated with IAV and LPS (IAV+LPS mice) exhibited cerebral microhemorrhage and vasogenic edema, which suggested that the BBB in these animals was impaired. However, there was no evidence of IAV in CNS parenchymal cells as well as the cerebral vascular endothelium in these mice. Therefore, the mechanism of impaired BBB function remains to be elucidated. The enhanced vascular damage and neuropathogenicity observed in IAV+LPS mice were suggested to be due to elevated production of plasma inflammatory cytokines in Chapter 1. Inflammatory cytokines can affect BBB permeability via apoptosis of vascular endothelial cells and vulnerability of TJ, as described above. Here, as the pathological mechanism of vasogenic CNS damage, these mechanisms were postulated and investigated. The results suggest that apoptosis of endothelial cells and astrocytes plays a significant role in the development of cerebral vascular damage in mice inoculated with IAV and LPS.

Materials and Methods

Virus, mice, and inoculations of IAV and LPS

IAV, mice and LPS used in this investigation were as described for Chapter 1. The experimental protocol for the murine model of IAE was also described for Chapter 1 (Fig. 1).

Terminal deoxynucleotidyl transferase-mediated dUTP nick end-labeling (TUNEL) method

DNA breaks in tissue sections were detected by TUNEL method, as previously described (Gavrieli *et al*, 1992). Briefly, 4 μm sections were dewaxed, hydrated, and washed with autoclaved distilled water. Sections were washed with autoclaved 0.01 M PBS and then incubated with 0.02 mg/ml proteinase K (Sigma) in 0.01 M PBS for 15 min at room temperature. To block endogenous peroxidase, the sections were treated with a solution of methanol containing 3% H_2O_2 for 15 min at room temperature. Sections were equilibrated with TdT buffer (Invitrogen, Carlsbad, CA) for 10 min and then incubated with a solution of 0.5 μM TdT (Invitrogen) and 10 μM biotin-16-dUTP (Roche Applied Science, Mannheim, Germany) in TdT buffer for 90 min at 37°C. Following this, the sections were incubated with peroxidase-conjugated-streptavidin (Nichirei Corp.) for 15 min. Labeled nuclei were detected by incubation in 0.05 M Tris-HCl buffer (pH 7.6) containing 0.02% DAB (Dojindo Laboratories), 0.005% H_2O_2 and 0.01 M

imidazole (Sigma). The sections were counterstained with methyl green. As a

positive control, tissue sections of the thymus from LPS-treated mice were

analyzed; these sections yielded tingible bodies typical of positive TUNEL

staining (data not shown). As an additional positive control, brain sections were

pretreated with 1 mg/ml DNAse I (Sigma) for 10 min at room temperature. After

washing, the sections were labeled as described above. As expected, pre-treatment

with DNAse I caused diffuse intense staining of cellular nuclei (data not shown).

IHC and double immunohistochemical staining

Serial sections were stained by the streptavidin-biotin immunoperoxidase

complex method using a Histofine SAB-PO kit (Nichirei Corp.). Briefly, sections

were dewaxed, hydrated, and then washed with 0.01 M PBS. To restore antigens,

the sections were treated with 0.01 M citrate buffer (pH 6.0) for 10 min at 98°C in

a microwave processor (MI-77; Azumaya, Tokyo, Japan). To block endogenous

peroxidase, the sections were quenched for 10 min at room temperature in a

solution of methanol containing 0.3% H_2O_2. The primary antibody was rabbit

anti-cleaved caspase 3, which recognizes the large fragment of activated caspase 3

resulting from cleavage adjacent to Asp175 (Wang *et al*, 2005) (1:500; Cell

Signaling Technology, Beverly, MA), rabbit anti-GFAP (1:3000; DAKO,

Carpentaria, CA), or rabbit anti-occludin (1:100; Invitrogen). Sections were

incubated with primary antibody for approximately 12 h at 4°C. The chromogenic

reaction was carried out in a solution of 0.05 M Tris-HCl buffer (pH 7.6)

36

containing 0.02% DAB, 0.005% H_2O_2, and 0.01 M imidazole. The sections were counterstained with methyl green or Mayer's hematoxylin. As a negative control, the primary antibody was replaced with 0.01 M PBS.

Double immunohistochemical staining was carried out to clarify the distribution of activated caspase 3 and GFAP. First, serial sections were stained with rabbit anti-activated caspase 3 antibody followed by Histofine SAB-PO. The chromogenic reaction was carried out in a solution of 0.05 M Tris-HCl buffer (pH 7.6) containing 0.02% DAB, 0.005% H_2O_2, and 0.01 M imidazole. The sections were then washed with 0.01 M PBS for 1.5 h at room temperature. After a blocking step, sections were incubated with rabbit anti-GFAP antibody, followed by biotin-conjugated goat anti-rabbit immunoglobulin secondary antibody (Nichirei Corp.) for 15 min at room temperature. The sections were treated with alkaline phosphatase-conjugated streptavidin (Nichirei Corp.) and then fast red II substrate (Nichirei Corp.). The sections were counterstained with methyl green and then mounted with a soluble encapsulating medium.

Quantification of TUNEL- or activated caspase 3-positive cells

To quantify the levels of *in situ* DNA breaks or caspase 3 activation, TUNEL- or activated caspase 3-positive cells in brain sections were counted. Briefly, 25 fields were randomly retrieved from the brain sections (18 fields from cerebrum sections and 7 fields from brain stem sections) at 200-fold magnification, and the number of positive cells was counted. The brains from IAV, LPS, and

IAV+LPS mice (n=3 in each group) were quantified. Results are expressed as means ± SEM. Differences were analyzed by the two-sided Student's *t*-test.

Western blot analysis

Brain pieces were homogenized by sonication in 5-times their volume of 2×SDS buffer (100 mM Tris-HCl, pH 6.8, 4% SDS, 30 mM EDTA, 15% glycerol). An aliquot was removed to quantify protein concentrations using a DC protein assay kit (Bio-Rad Laboratories, Hercules, CA). An equal volume of 2×reducing buffer (10% 2-mercaptoethanol, 0.06% bromophenol-blue) was added to the lysate (Olney *et al*, 2002). Samples were boiled for 5 min and stored at -70°C.

To identify activated caspase 3 or TJ-associated proteins, 100 μg of total protein was fractioned by sodium dodecyl sulfate-polyacrylamide gel electrophoresis (SDS-PAGE) on 15% or 7.5% acrylamide gels. The separated proteins were transferred to an Immobilon membrane (Millipore, Cork, Ireland). The membrane was incubated with primary antibodies for approximately 12 h at 4°C, followed by the appropriate horseradish peroxidase-conjugated secondary antibody (1:1500; Biosource, Camarillo, CA) for 1 h at room temperature. The following primary antibodies were used, as indicated: rabbit anti-cleaved caspase 3 (Asp175) (1:1000; Cell Signaling Technology), rabbit anti-occludin (1:1000; Invitrogen), mouse anti-zona occludin (ZO)-1 (1:1000; Invitrogen), and mouse anti-α-tubulin (B-5-1-2) as an internal control (1:3000; Sigma). Immunoreactive proteins were detected using ECL Western blotting detection reagents (GE

Healthcare, Buckinghamshire, UK), and signals were detected using a LAS-4000 mini-luminescent image analyzer (GE Healthcare). Signal intensities were analyzed using ImageQuant TL software (GE Healthcare).

Results

Increase of TUNEL-positive cells

The apoptosis of the brain was analyzed with TUNEL method, morphology of nuclei, and activation of caspase 3 in this examination. The brains of the IAV, LPS, and IAV+LPS groups were submitted to TUNEL method analysis at 24, 48, and 72 h after the LPS inoculations. Very few nuclei that were positive for TUNEL were present in the brains of the IAV groups. Meanwhile, there were relatively large numbers of positively-labeled cells in the cerebral parenchyma of the LPS and IAV+LPS groups. In these animals, cells with TUNEL-positive nuclei were located mostly around blood vessels (Fig. 14). The number of TUNEL-positive cells in the brains of the IAV, LPS, and IAV+LPS groups was quantified 24, 48, and 72 h after LPS inoculation (Fig. 17A). TUNEL-positive cells were significantly elevated in the IAV+LPS group (1.76±0.14) as compared to the IAV and LPS groups (0.62±0.02 and 0.81±0.06, respectively) 24 h after LPS inoculation. The number of TUNEL-positive cells in the IAV+LPS group reached a peak at 48 h (1.96±0.35), and then decreased to the same level as the IAV group 72 h after LPS inoculation (0.68±0.03).

Detection of activated caspase 3

In the LPS and IAV+LPS groups, there were scattered neural parenchymal cells that were positive for activated caspase 3 in the cytoplasm and nuclei. Activated caspase 3-positive cells were distributed mainly in the cerebral cortex and brain stem. Numerous positive cells were located around cerebral capillaries (Fig. 15) and had pyknotic round-to-oval nuclei. A small number of spindle-shaped cells located in the capillary walls were also positive for activated caspase 3 (Fig. 16). Caspase 3-positive cells in the brains of the LPS and IAV+LPS groups were quantified 24, 48, and 72 h after LPS inoculation (Fig. 17B). Similar to TUNEL positive-cells (Fig. 17A), the number of caspase 3-positive cells was significantly higher in the IAV+LPS group (0.92±0.10) than the LPS group (0.53±0.05) 24 h after LPS inoculation. The number of activated caspase 3-positive cells peaked at 24 h, and then decreased 48 h (0.75±0.09) and 72 h (0.36±0.06) after LPS inoculation. This increase in activated caspase 3-positive cells was also suggested by Western blot analysis (Fig. 17C). Activated caspase 3 signals (17 and 19 kDa) were more intense in the brain of IAV+LPS mice at 24 and 48 h after LPS inoculation, compared to the brain of negative control (saline-inoculated mice), IAV, and LPS mice.

Increased GFAP-positive astrocytes and colocalization of activated caspase 3 and GFAP

In the cerebrums of mice in the IAV group, GFAP-positive cells were observed mainly in the white matter and submeningeal regions (Fig. 18). There were a small number of GFAP-positive astrocytes in the gray matter of the cerebral cortex, except in the circumferences of blood vessels. In the cerebrum of the LPS and IAV+LPS group, GFAP-positive staining of astrocytes was low 6 h after LPS inoculation (Fig. 19), and then increased in a diffuse manner in the cerebral gray matter 48 h after LPS inoculation (Fig. 20). There were no obvious differences in the intensity and distribution of GFAP-positive staining between the LPS and IAV+LPS groups 48 h after LPS inoculations.

Cells that were positive for TUNEL and activated caspase 3 tended to be distributed in the cerebral parenchyma around the blood vessels. To identify these apoptotic cells, brain sections were double-stained for activated caspase 3 and GFAP (Fig. 21). Most of the cells that were positive for activated caspase 3 (brown color) were negative for GFAP (red color), but some of the activated caspase 3-positive cells were positive for GFAP (reddish brown).

Expression levels of TJ proteins in experimental animals

The expression levels of TJ proteins were measured by IHC and Western blot. IHC revealed that occludin-positive staining localized to the cytoplasm of most cerebral endothelial cells in the IAV group (Fig. 22). In this group, the cerebral endothelium exhibited smooth, homogenous positive staining. In the LPS and IAV+LPS group, a similar pattern of positive occludin staining was observed

41

in the cerebral endothelium 6 h after LPS inoculation. However, for both groups, at 24 and 48 h after LPS inoculation, when cerebral endothelia exhibited microhemorrhage, disrupted and granular occludin-positive signals were observed (Fig. 23).

The expression levels of occludin (60 kDa) and ZO-1 (220 kDa) were also analyzed by Western blot in the brain of control, IAV, LPS, and IAV+LPS groups at 6 and 48 h after LPS inoculation (Fig. 24A). The signal intensities of occludin and ZO-1 were analyzed using ImageQuant TL software. The levels of both proteins by 3-times calculation were nearly identical in the IAV, LPS, and IAV+LPS groups (n=3; Fig. 24B).

Fig. 14.   Brain, mouse, the IAV+LPS group, 48 h after LPS inoculations. The nuclei positive for DNA fragmentation are distributed in and around blood vessels (arrows). Bar = 100 μm. TUNEL method, methyl green counterstain. The reaction product was visualized with the streptavidin-biotin immunoperoxidase complex method.

Fig. 15.   Brain, mouse, the IAV+LPS group, 24 h after LPS inoculations. The cells positive for activated caspase 3 are distributed around blood vessels (arrows). Bar = 100 μm. IHC (activated caspase 3) by the streptavidin-biotin immunoperoxidase complex method, methyl green conterstain.

Fig. 16.   Brain, mouse, the IAV+LPS group, 24 h after LPS inoculations. A vascular endothelial cell shows positive reaction for activated caspase 3 (arrow). Bar = 50 μm. IHC (activated caspase 3) by the streptavidin-biotin immunoperoxidase complex method, methyl green conterstain.
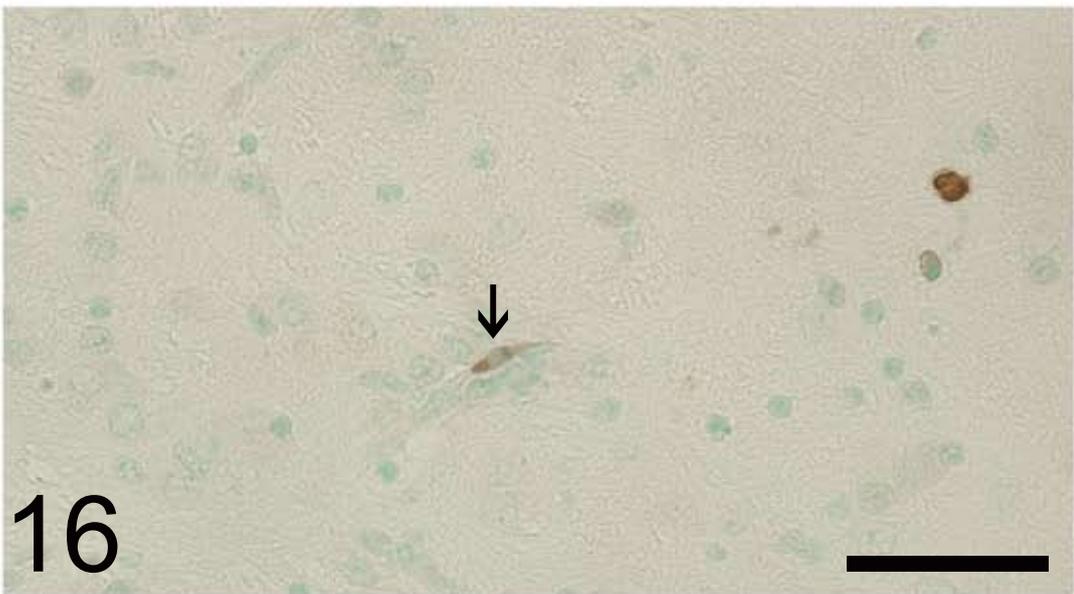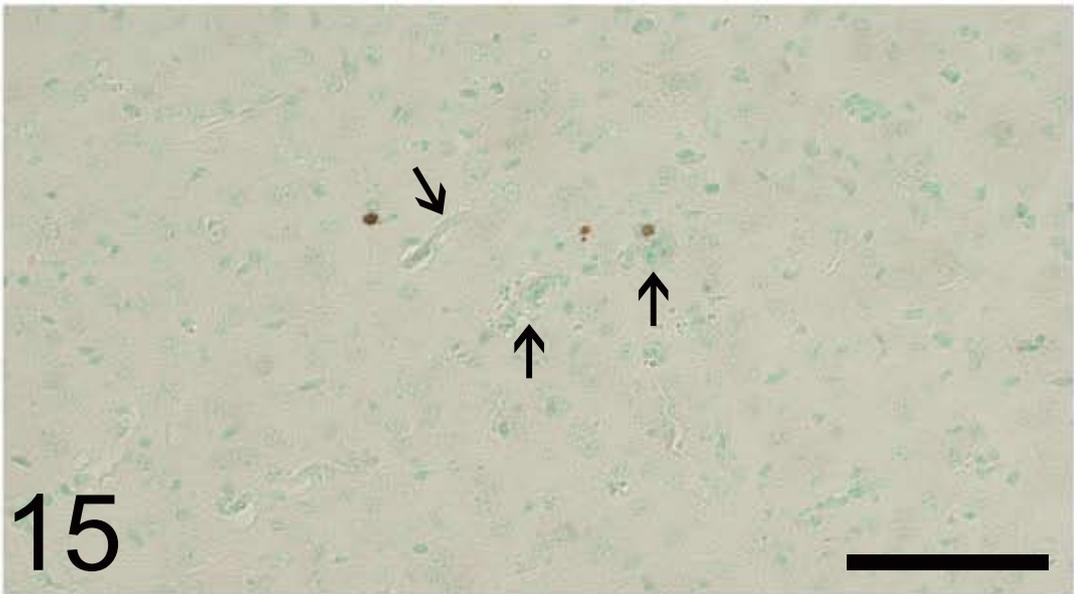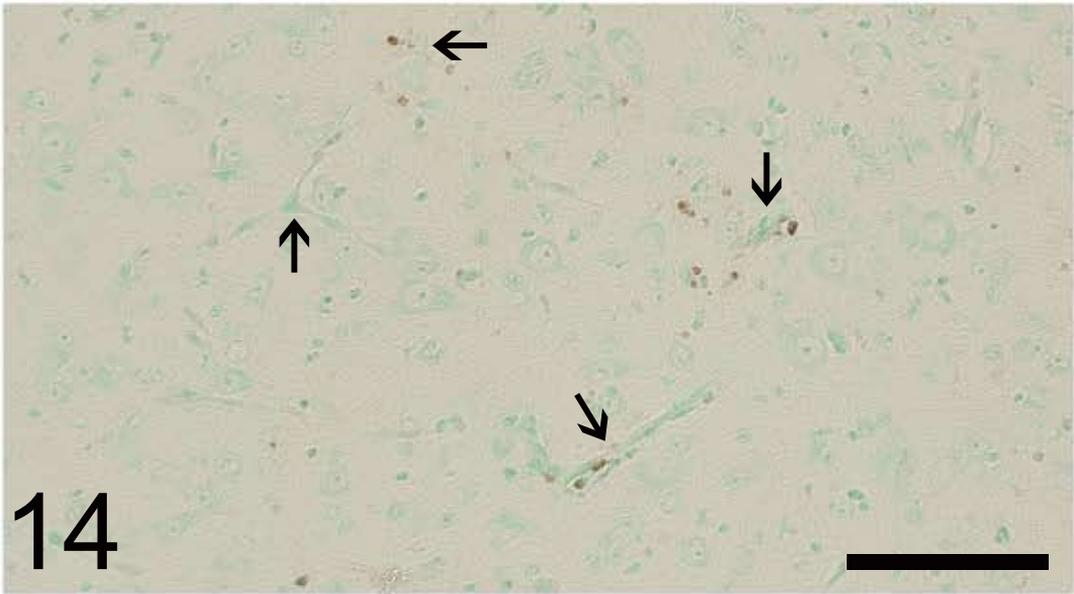
Fig. 17. (A) The number of TUNEL- positive cells per field in the brains. The brains of the IAV (open column), LPS (striped column), and IAV+LPS (filled column) groups were collected at 24, 48, and 72 h after LPS inoculations. (B) The number of activated caspase 3-positive cells per field in brains. The brains of the LPS (striped column) and IAV+LPS (filled column) groups were collected at 24, 48, and 72 h after LPS inoculations. The values are expressed as the average numbers of positive cells in a field of 200-fold magnification after counting 25 fields. In each group, 4 samples were subjected to the analyses. Error bars mean standard error. The statistical difference was determined by two-sided Student's *t*-test (* $P < 0.01$, ** $P < 0.05$). (C) Western blot analysis of activated caspase 3 in the brain (top column). The brains were collected from the control, IAV, LPS, and IAV+LPS groups at 24 and 48 h after LPS inoculations. Anti α-tubulin antibody was used as an internal control (bottom column).

A — TUNEL-positive cells

B — Activated caspase 3-positive cells

C — activated caspase 3 / α-tubulin western blot

Fig. 18.　Brain, mouse, the IAV group, 24 h after saline inoculations (5 dpi). Positive reactions for GFAP are localized in circumferences of blood vessels and the white matter. Only a few positive cells are observed in the cerebral cortex. Bar = 100 μm. IHC (GFAP) by the streptavidin-biotin immunoperoxidase complex method, Mayer's hematoxylin conterstain.

Fig. 19.　Brain, mouse, the IAV+LPS group, 6 h after LPS inoculations. Positive cells for GFAP are mainly localized in circumferences of blood vessels and the white matter, like the brain of the IAV group (Fig. 18). Bar = 100 μm. IHC (GFAP) by the streptavidin-biotin immunoperoxidase complex method, Mayer's hematoxylin conterstain.

Fig. 20.　Brain, mouse, the IAV+LPS group, 48 h after LPS inoculations. Positive cells for GFAP are diffusely distributed in the cerebral parenchyma as well as circumferences of blood vessels and the white matter. Bar = 100 μm. IHC (GFAP) by the streptavidin-biotin immunoperoxidase complex method, Mayer's hematoxylin conterstain.

18

19

20

Fig. 21. Brain, mouse, the IAV+LPS group, 6 h after saline inoculations. Double IHC for GFAP (red) and activated caspase 3 (brown). Positive reaction for GFAP appears beside the blood vessel (arrow). The cell positive for activated caspase 3 is negative for GFAP (filled arrowhead) or positive for GFAP (open arrowhead; reddish brown). Bar = 25 μm. The streptavidin-biotin alkaline phosphatase complex method for GFAP; the streptavidin-biotin immunoperoxidase complex method for activated caspase 3; methyl green conterstain.

Fig. 22. Brain, mouse, the IAV group, 24 h after saline inoculations. Positive reactions for occludin are seen in the vascular endothelium. The pattern of positive staining is smooth and linear. Bar = 50 μm. IHC (occludin) by the streptavidin-biotin immune-peroxidase complex method, Mayer's hematoxylin conterstain.

Fig. 23. Brain, mouse, the IAV+LPS group, 48 h after LPS inoculations. The endothelium with microhemmorage shows granular positive reaction for occludin (arrowheads). The arrow indicates the erythrocytes leaking from blood vessels. Bar = 50 μm. IHC (occludin) by the streptavidin-biotin immunoperoxidase complex method, Mayer's hematoxylin conterstain.
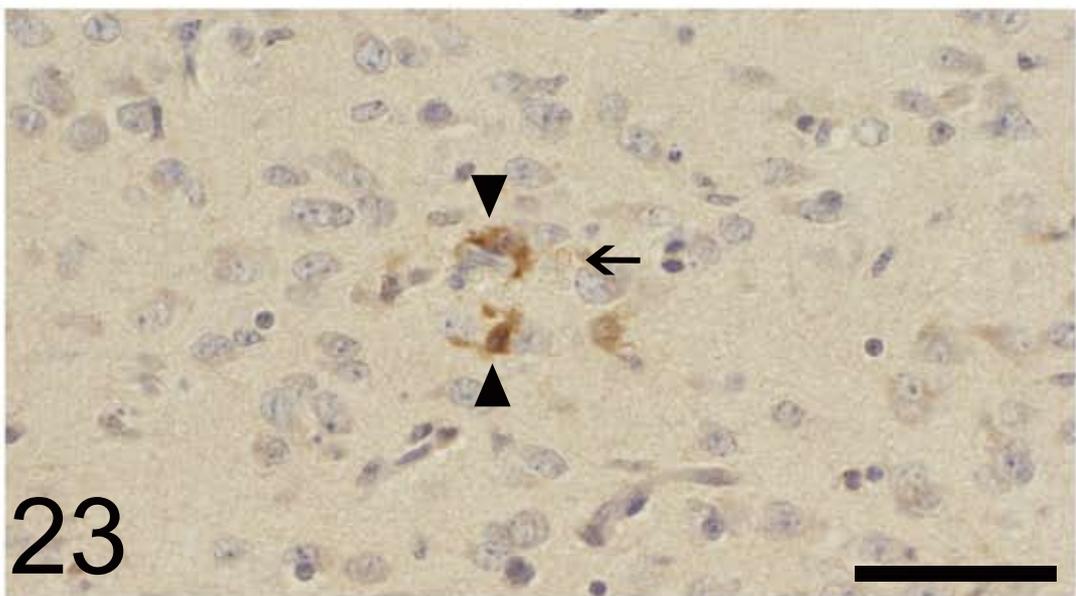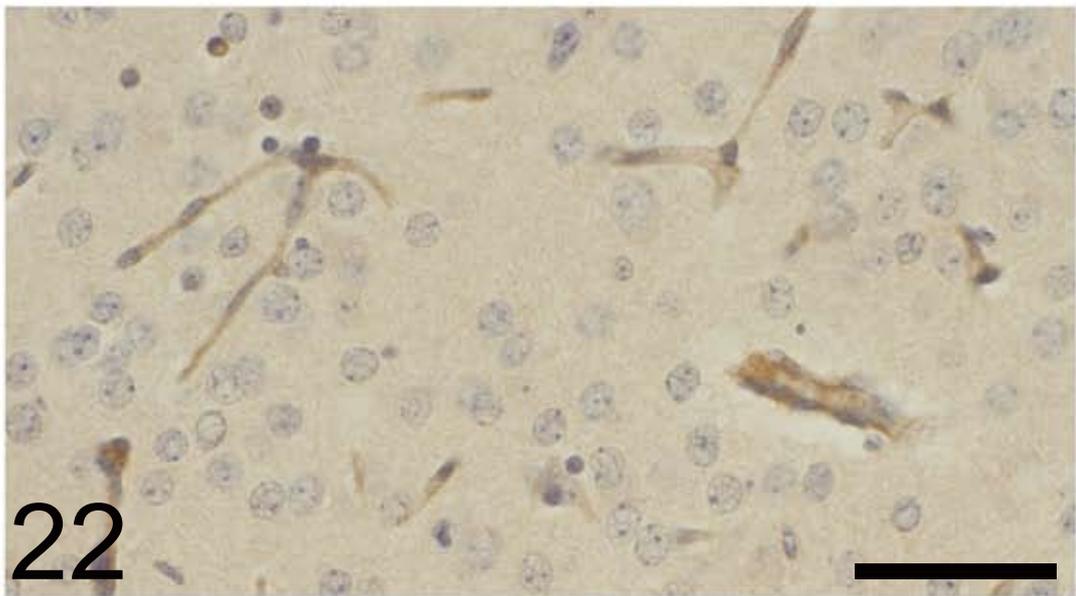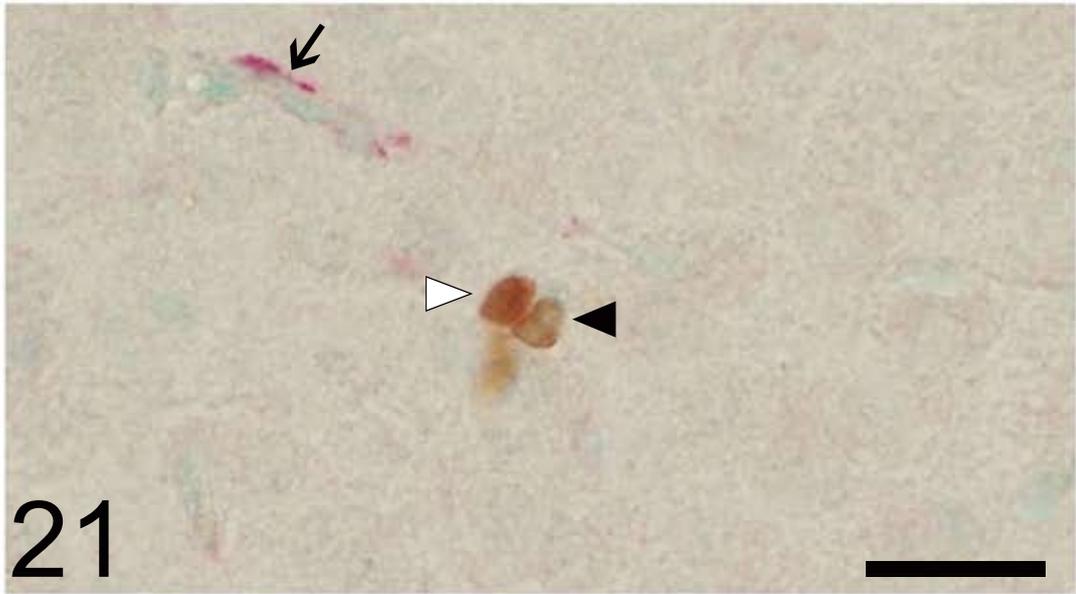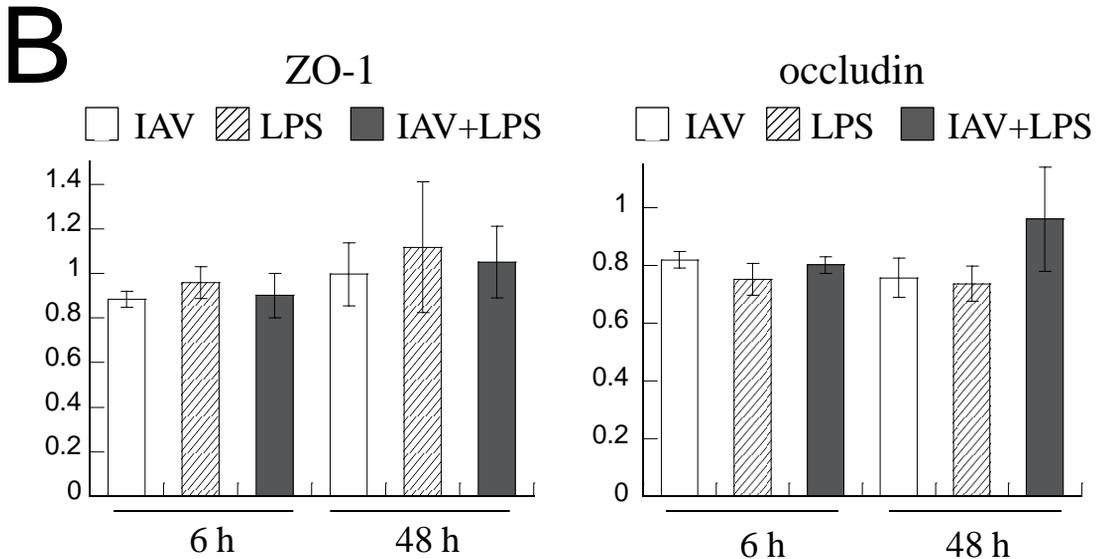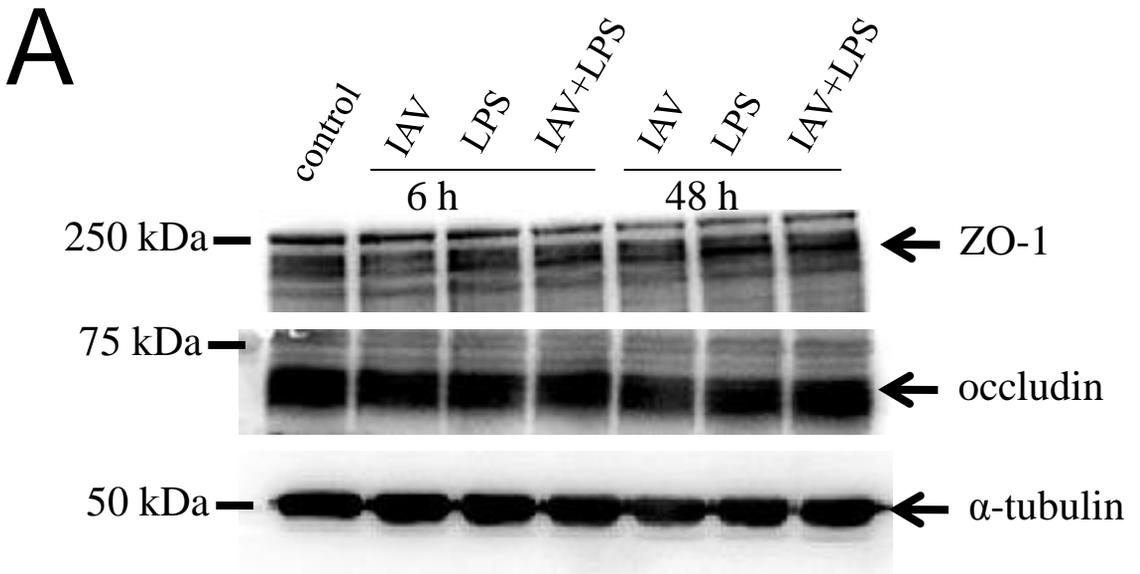
Fig. 24. The expression levels of TJ proteins. (A) Western blot analysis of ZO-1 (top column) and occludin (middle column) in the brain. The brains were collected from the control, IAV, LPS, and IAV+LPS groups at 6 and 48 h after LPS inoculations. Anti α-tubulin antibody was used as an internal control (bottom column). (B) Comparison of signal intensities for ZO-1 (left) and occludin (right) in the brain. Values are expressed as relative strengths of signals vs. the control. The analysis was performed 3 times. There are no significant difference between values by Student's *t*-test. Each error bar means standard error.

51

Discussion

Chapter 1 demonstrated that pulmonary IAV infection enhances LPS-induced encephalopathy and elevates plasma inflammatory cytokines in neonatal ICR mice. In the brains of these animals, scattered microhemorrhage and vasogenic brain edema were observed histopathologically. Here, an investigation was carried out in order to clarify the pathological mechanism of cerebral vascular damage leading to IAE-like encephalopathy in IAV+LPS mice.

In previous reports, LPS in the bloodstream has been shown to induce apoptosis in endothelial cells directly, or through induction of TNF-α and other cytokines (Choi *et al*, 1998; Hull *et al*, 2002). It has also been reported that apoptosis of the vascular endothelium plays an important role in LPS-induced pathogenicity (Haimovitz-Friedman *et al*, 1997). In this chapter, the number of TUNEL-positive cells in the brains of the LPS and IAV+LPS groups increased 24-48 h after LPS inoculation as compared to the IAV group. Moreover, TUNEL-positive cells in the IAV+LPS group were more abundant than in the LPS group. Most TUNEL-positive cells had round, pyknotic nuclei, which was consistent with characteristic nuclear morphology of apoptotic cells. Activated caspase 3 was also detected in the brains of these mice, providing further support for the induction of apoptosis as an underlying component of the pathological mechanism of IAE-like encephalopathy in IAV+LPS mice. Caspase 3, an effector caspase that is activated through various signaling pathways, causes proteolytic

cleavage of many DNA fragmentation-inducing proteins, such as poly ADP ribose polymerase (Rath and Aggarwal, 1999). The number of activated caspase 3-positive cells also tended to be higher in the IAV+LPS group than the LPS group, and peaked earlier than the number of TUNEL-positive cells. These results suggest that apoptosis in the brains of IAV+LPS mice was more severe than in the other groups. This is consistent with the differences in the appearance of CNS lesions and BBB permeability among the three groups.

Most of the cells that were positive for TUNEL and activated caspase 3 were distributed in and around the vascular walls. Some of the activated caspase 3-positive cells exhibited an endothelial-like spindle appearance, or were double-positive for GFAP, an intermediate filament protein and a marker of astrocytes. These results suggest that treatment of neonatal mice with IAV and LPS induces apoptosis of vascular endothelial cells and astrocytes in the brain. Astrocytes are closely adjacent to the outer surface of the vascular endothelium, and contribute to the strength and structural integrity of the BBB (Abbott, 2002; Eng et al, 2000; Kacem et al, 1998; Pekny et al, 1998). Thus, the induction of apoptosis in astrocytes as well as vascular endothelial cells may contribute to the increased BBB permeability observed in IAV+LPS mice.

The BBB is a complex cellular system (Petty and Lo, 2002). Passage of blood-borne molecules across the BBB can occur in a transcellular or paracellular manner. The latter pathway is almost completely obstructed by TJ, and consequently, functional disruption of TJ can lead to brain edema. Occludin is a

transmembrane protein of TJ and contributes to selective permeability (Balda *et al*, 2000; Tsukita *et al*, 2001). ZO-1 is a cytoplasmic accessory protein that binds directly to occludin and claudins, another transmembrane protein. ZO-1 supports the structural integrity of the barrier formed by occludin and claudins (Itoh *et al*, 1999). In previous reports, the expression levels of these TJ proteins have been shown to be altered by LPS stimulation and inflammatory cytokines, such as TNF-α, IL-1β, and IL-6 (Han *et al*, 2004; Harkness *et al*, 2000; Petty and Lo, 2002; Schulze *et al*, 1997). In the current study, the distribution of occludin was granular and non-continuous in the impaired endothelium of the IAV+LPS group. However, Western blot analysis indicated that there was no decrease in the expression levels of occludin and ZO-1 in the brains of these mice. There was evidence of neutrophilic infiltration to cerebral parenchyma of the LPS and IAV+LPS group, but infiltration of neutrophils is not likely to affect BBB permeability, unlike lymphocytes and macrophages (Burns *et al*, 2000). These results suggest that an increase in paracellular passage due to degradation of TJ were not the cause of increased BBB permeability observed in the IAV+LPS mice.

GFAP-positive staining increased in a diffuse manner with time in the brains of the IAV+LPS group. Upregulation of GFAP expression is an early response of astrocytes to various CNS insults, including cryogenic lesions, stab wounds, experimental allergic encephalomyelitis, and Alzheimer's disease (Eddleston and Mucke, 1993; Eng *et al*, 2000). Increased GFAP expression is an important step in astrocyte activation, and is considered to be a sensitive and early

biomarker of neurotoxicity (Eng *et al*, 2000; Pekny and Pekna, 2004). The results indicate that the IAE-like encephalopathy induced by combined treatment with IAV and LPS was initiated by damage to the vascular endothelium and astrocytes, and extended diffusely in the brains of IAV+LPS mice.

Previous reports have described the apoptosis of systemic vascular endothelial cells and CNS resident cells, including glial cells and neurons, in patients with IAE (Morishima *et al*, 2002; Nakai *et al*, 2003; Nunoi *et al*, 2005), and apoptosis of these cells is believed to play a role in the development of IAE. To date, increased paracellular permeability of the BBB through degradation of TJ has not been implicated in the development of IAE. In the current study, apoptosis was induced in the CNS in neonatal mice treated with a combination of IAV and LPS. Thus, our murine model of IAE involves a similar mechanism of increased permeability of the BBB as IAE in humans.

Chapter 1 described the hyper-induction of inflammatory cytokines in the peripheral blood of mice treated with IAV and LPS. The production of inflammatory cytokines preceded the appearance of neuropathological changes in these mice, and cytokine concentrations correlated positively with the severity of CNS lesions. High concentrations of inflammatory cytokines in the blood induce apoptosis of vascular endothelial cells and resident CNS cells (Mohler *et al*, 1993; Reyes *et al*, 2009; Takuma *et al*, 2004; Yuan and Yankner, 2000). Taken together, these results indicate that apoptosis induced by elevated inflammatory cytokines contributes to the IAE-like encephalopathy of neonatal IAV+LPS mice.

Summary

The results reported in Chapter 1 demonstrated that pulmonary IAV infection enhances LPS-induced encephalopathy and induces elevated concentrations of plasma inflammatory cytokines in neonatal mice. Histopathologically, the neonatal mice exhibited an IAE-like vasogenic encephalopathy. However, the underlying neuropathological mechanism of disease progression was not elucidated. In the current chapter, the numbers of TUNEL- and activated caspase 3-positive cells were increased in the brains of IAV+LPS mice. Some of the activated caspase 3-positive cells had an endothelial cell-like shape, and some were immunohistochemically positive for GFAP. These results suggest that apoptosis of vascular endothelial cells and astrocytes is elevated in the brains of IAV+LPS mice. Although TJ were morphologically impaired, the expression of TJ proteins was not altered in the IAV+LPS group. Overall, these results suggest that the impaired permeability of the BBB and resultant IAE-like encephalopathy in IAV+LPS mice is due to increased apoptosis of vascular endothelial cells and astrocytes in the brain. Apoptosis of these cells induced by hypercytokinemia is believed to play a significant role in the development of IAE. Thus, the pathological mechanism of development of brain lesions in mice treated with IAV and LPS might be similar to that of IAE. Furthermore, hypercytokinemia could be a crucial causative factor in the development of encephalopathies in the current murine model as well as IAE in humans.

General conclusion

Influenza virus-associated encephalopathy (IAE) is a highly lethal neural complication of influenza virus infection that mostly affects children aged 2-4 years. The characteristic clinical finding of IAE is acute symmetric brain edema after the onset of flu-related fever. The brain edema is often followed by DIC and multiple organ failure. Histopathological analysis has revealed that the encephalopathy is accompanied by BBB dysfunction due to an impairment of vascular endothelial cells. Therefore, the essential component of IAE is considered to be a rapid onset of vascular disorder. However, the pathological mechanism of IAE is still unknown and there is no animal model of IAE. Direct infection of the CNS by influenza virus is not considered to be the cause of IAE, since the virus is not detected in the CNS of most IAE patients. On the other hand, elevated inflammatory cytokines, such as TNF-α, IL-1β, and IL-6, have been observed in the serum of IAE patients, which has led to the suggestion that hypercytokinemia is the cause of the encephalopathy.

In Chapter 1, neonatal ICR mice treated with a combination of IAV and LPS, and the accompanying brain lesions were investigated as a candidate experimental model of IAE. Infection with pulmonary IAV exacerbated the neuropathogenicity of LPS inoculation, and increased BBB permeability. In addition, IAV infection enhanced LPS-induced production of inflammatory cytokines in the blood. Cerebral microscopic changes in the brains of mice

inoculated with IAV and LPS were characterized by scattered microhemorrhage and hyaline droplet formation in the peripheries of blood vessels. These findings suggested that the CNS damage in these mice was caused by cerebral vascular damage. Importantly, the histopathology of IAV+LPS mice was similar to IAE. Plasma levels of TNF-α and IL-6 were significantly increased in IAV+LPS mice, which was also consistent with IAE in humans. Moreover, IAV was not detected in the brains of these animals. These results suggested that combined treatment with IAV and LPS induces an IAE-like encephalopathy in neonatal mice.

In Chapter 2, the pathological mechanism of the IAE-like encephalopathy induced in IAV+LPS mice was examined. Apoptosis of vascular endothelial cells and astrocytes was elevated in the brains of IAV+LPS mice as compared to mice treated with IAV or LPS alone. Since astrocytes and vascular endothelial cells contribute to the integrity and function of the BBB, apoptotic damage of these cells would likely affect BBB permeability. Western blot analysis demonstrated that the expression levels of TJ proteins were unaltered, although TJ were morphologically impaired, based on IHC. These results suggested that impairment of the BBB and the resultant IAE-like encephalopathy in IAV+LPS mice is caused by apoptosis of vascular endothelial cells and astrocytes in the brain, and that increased paracellular permeability regulated by TJ proteins is not related to the neuropathogenicity. Previous reports have suggested that apoptosis of CNS resident cells and vascular endothelial cells plays an important role in the development of IAE. Thus, the pathological mechanism of increased permeability

of the BBB in neonatal mice treated with IAV and LPS appears to be similar to that of IAE in humans.

In conclusion, pulmonary infection of neonatal ICR mice by IAV enhanced LPS-induced encephalopathy and elevated the concentrations of plasma inflammatory cytokines. Encephalopathy in mice treated with IAV and LPS shared similar characteristics with IAE in terms of CNS lesions, the dynamics of inflammatory cytokines, and the absence of direct IAV infection of the CNS. Moreover, apoptosis of astrocytes and vascular endothelial cells may contribute to the IAE-like encephalopathy of mice treated with IAV and LPS. These results suggest that both encephalopathies in IAE and in our murine model induced by a combined of IAV and LPS have a similar pathological mechanism of increased BBB permeability. Moreover, hypercytokinemia is likely to be a crucial causative factor in the encephalopathies of the present murine model and IAE in humans. The murine model established in the current study will be useful in the development of strategies for early diagnosis and treatment of IAE.

References

Abbott N (2002). Astrocyte-endothelial interactions and blood-brain barrier permeability. *J Anat* **200:** 629-38.

Aiba H, Mochizuki M, Kimura M, Hojo H (2001). Predictive value of serum interleukin-6 level in influenza virus-associated encephalopathy. *Neurology* **57:** 295-9.

Akira S, Uematsu S, Takeuchi O (2006). Pathogen recognition and innate immunity. *Cell* **124:** 783-801.

Alexander J, Jacob A, Cunningham P, Hensley L, Quigg R (2008). TNF is a key mediator of septic encephalopathy acting through its receptor, TNF receptor-1. *Neurochem Int* **52:** 447-56.

Balda M, Flores-Maldonado C, Cereijido M, Matter K (2000). Multiple domains of occludin are involved in the regulation of paracellular permeability. *J Cell Biochem* **78:** 85-96.

Banks W (2009). Characteristics of compounds that cross the blood-brain barrier. *BMC Neurol* **9 Suppl 1:** S3.

Beutler B, Rietschel E (2003). Innate immune sensing and its roots: the story of endotoxin. *Nat Rev Immunol* **3:** 169-76.

Bigdeli M, Khoshbaten A (2008). In vivo preconditioning with normobaric hyperoxia induces ischemic tolerance partly by triggering tumor necrosis factor-alpha converting enzyme/tumor necrosis factor-alpha/nuclear factor-kappaB. *Neuroscience* **153:** 671-8.

Bogdanski R, Blobner M, Becker I, Hänel F, Fink H, Kochs E (2000). Cerebral histopathology following portal venous infusion of bacteria in a chronic porcine model. *Anesthesiology* **93:** 793-804.

Burns A, Bowden R, MacDonell S, Walker D, Odebunmi T, Donnachie E, Simon S, Entman M, Smith C (2000). Analysis of tight junctions during neutrophil transendothelial migration. *J Cell Sci* **113:** 45-57.

Centers for Disease Control and Prevention (2009). Neurologic complications associated with novel influenza A (H1N1) virus infection in children - Dallas, Texas, May 2009. *MMWR Morb Mortal Wkly Rep* **58:** 773-8.

Chen H, Smith GJD, Zhang SY, Qin K, Wang J, Li KS, Webster RG, Peiris JSM, Guan Y (2005). H5N1 virus outbreak in migratory waterfowl. *Nature* **436:** 191-192.

Choi K, Wong F, Harlan J, Chaudhary P, Hood L, Karsan A (1998). Lipopolysaccharide mediates endothelial apoptosis by a FADD-dependent pathway. *J Biol Chem* **273:** 20185-8.

Diaz A, Chepenik K, Korn J, Reginato A, Jimenez S (1998). Differential regulation of cyclooxygenases 1 and 2 by interleukin-1 beta, tumor necrosis factor-alpha, and transforming growth factor-beta 1 in human lung fibroblasts. *Exp Cell Res* **241:** 222-9.

Eddleston M, Mucke L (1993). Molecular profile of reactive astrocytes--implications for their role in neurologic disease. *Neuroscience* **54:** 15-36.

Eng L, Ghirnikar R, Lee Y (2000). Glial fibrillary acidic protein: GFAP-thirty-one years (1969-2000). *Neurochem Res* **25:** 1439-51.

Fukui S, Fazzina G, Amorini AM, Dunbar JG, Marmarou A (2003). Differential effects of atrial natriuretic peptide on the brain water and sodium after experimental cortical contusion in the rat. *Journal of Cerebral Blood Flow and Metabolism* **23:** 1212-1218.

Gavrieli Y, Sherman Y, Ben-Sasson S (1992). Identification of programmed cell death in situ via specific labeling of nuclear DNA fragmentation. *J Cell Biol* **119:** 493-501.

Haimovitz-Friedman A, Cordon-Cardo C, Bayoumy S, Garzotto M, McLoughlin M, Gallily R, Edwards Cr, Schuchman E, Fuks Z, Kolesnick R (1997). Lipopolysaccharide induces disseminated endothelial apoptosis requiring ceramide generation. *J Exp Med* **186:** 1831-41.

Han J, Brown T, Beutler B (1990). Endotoxin-responsive sequences control cachectin/tumor necrosis factor biosynthesis at the translational level. *J Exp Med* **171:** 465-75.

Han X, Fink MP, Yang R, Delude RL (2004). Increased iNOS activity is essential for intestinal epithelial tight junction dysfunction in endotoxemic mice. *Shock* **21:** 261-70.

Harkness K, Adamson P, Sussman J, Davies-Jones G, Greenwood J, Woodroofe M (2000). Dexamethasone regulation of matrix metalloproteinase expression in CNS vascular endothelium. *Brain* **123:** 698-709.

Hirano A (1991). Neurons and Astrocytes. In: *Textbook of Neuropathology*, 2nd ed., pp. 1-94., Davis RL and Robertson DM eds., Williams & Willkins. Baltimore, USA.

Huang Y, Lin T, Wu S, Tsao K (2003). Influenza A-associated central nervous system dysfunction in children presenting as transient visual hallucination. *Pediatr Infect Dis J* **22:** 366-8.

Hull C, McLean G, Wong F, Duriez P, Karsan A (2002). Lipopolysaccharide signals an endothelial apoptosis pathway through TNF receptor-associated factor 6-mediated activation of c-Jun NH2-terminal kinase. *J Immunol* **169:** 2611-8.

Ichiyama T, Isumi H, Ozawa H, Matsubara T, Morishima T, Furukawa S (2003). Cerebrospinal fluid and serum levels of cytokines and soluble tumor necrosis factor receptor in influenza virus-associated encephalopathy. *Scand J Infect Dis* **35:** 59-61.

Isoda N, Sakoda Y, Kishida N, Bai G, Matsuda K, Umemura T, Kida H (2006). Pathogenicity of a highly pathogenic avian influenza virus, A/chicken/Yamaguchi/7/04 (H5N1) in different species of birds and mammals. *Arch Virol* **151:** 1267-79.

Ito Y, Ichiyama T, Kimura H, Shibata M, Ishiwada N, Kuroki H, Furukawa S, Morishima T (1999). Detection of influenza virus RNA by reverse transcription-PCR and proinflammatory cytokines in influenza-virus-associated encephalopathy. *J Med Virol* **58:** 420-5.

Itoh M, Furuse M, Morita K, Kubota K, Saitou M, Tsukita S (1999). Direct binding of three tight junction-associated MAGUKs, ZO-1, ZO-2, and ZO-3, with the COOH termini of claudins. *J Cell Biol* **147:** 1351-63.

Jakeman K, Rushton D, Smith H, Sweet C (1991). Exacerbation of bacterial toxicity to infant ferrets by influenza virus: possible role in sudden infant death syndrome. *J Infect Dis* **163:** 35-40.

Janssens S, Burns K, Vercammen E, Tschopp J, Beyaert R (2003). MyD88S, a splice variant of MyD88, differentially modulates NF-kappaB- and AP-1-dependent gene expression. *FEBS Lett* **548:** 103-7.

Julkunen I, Melén K, Nyqvist M, Pirhonen J, Sareneva T, Matikainen S (2000). Inflammatory responses in influenza A virus infection. *Vaccine* **19 Suppl 1:** S32-7.

Kacem K, Lacombe P, Seylaz J, Bonvento G (1998). Structural organization of the perivascular astrocyte endfeet and their relationship with the endothelial glucose transporter: a confocal microscopy study. *Glia* **23:** 1-10.

Kawai T, Akira S (2006). TLR signaling. *Cell Death Differ* **13:** 816-25.

Kumai Y, Ooboshi H, Takada J, Kamouchi M, Kitazono T, Egashira K, Ibayashi S, Iida M (2004). Anti-monocyte chemoattractant protein-1 gene therapy protects against focal brain ischemia in hypertensive rats. *J Cereb Blood Flow Metab* **24:** 1359-68.

Li Z, Hulderman T, Salmen R, Chapman R, Leonard S, Young S, Shvedova A, Luster M, Simeonova P (2007). Cardiovascular effects of pulmonary exposure to single-wall carbon nanotubes. *Environ Health Perspect* **115:** 377-82.

Lin C, Tsai C, Cheng C, Chen Y, Tournier F, Yeh T (2007). Expression of Toll-like receptors in cultured nasal epithelial cells. *Acta Otolaryngol* **127:** 395-402.

Lu Y, Yeh W, Ohashi P (2008). LPS/TLR4 signal transduction pathway. *Cytokine* **42:** 145-51.

Lundemose J, Smith H, Sweet C (1993). Cytokine release from human peripheral blood leucocytes incubated with endotoxin with and without prior infection with influenza virus: relevance to the sudden infant death syndrome. *Int J Exp Pathol* **74:** 291-7.

Matsuda K, Park C, Sunden Y, Kimura T, Ochiai K, Kida H, Umemura T (2004). The vagus nerve is one route of transneural invasion for intranasally inoculated influenza a virus in mice. *Vet Pathol* **41:** 101-7.

Merrill J, Benveniste E (1996). Cytokines in inflammatory brain lesions: helpful and harmful. *Trends Neurosci* **19:** 331-8.

Mohler K, Torrance D, Smith C, Goodwin R, Stremler K, Fung V, Madani H, Widmer M (1993). Soluble tumor necrosis factor (TNF) receptors are effective therapeutic agents in lethal endotoxemia and function simultaneously as both TNF carriers and TNF antagonists. *J Immunol* **151:** 1548-61.

Morgan E, Varro R, Sepulveda H, Ember J, Apgar J, Wilson J, Lowe L, Chen R, Shivraj L, Agadir A, Campos R, Ernst D, Gaur A (2004). Cytometric bead array: a multiplexed assay platform with applications in various areas of biology. *Clin Immunol* **110:** 252-66.

Morishima T, Togashi T, Yokota S, Okuno Y, Miyazaki C, Tashiro M, Okabe N, (2002). Encephalitis and encephalopathy associated with an influenza epidemic in Japan. *Clin Infect Dis* **35:** 512-7.

Mosser D, Zhang X (2008). Interleukin-10: new perspectives on an old cytokine. *Immunol Rev* **226:** 205-18.

Nain M, Hinder F, Gong J, Schmidt A, Bender A, Sprenger H, Gemsa D (1990). Tumor necrosis factor-alpha production of influenza A virus-infected macrophages and potentiating effect of lipopolysaccharides. *J Immunol* **145:** 1921-8.

Nakai Y, Itoh M, Mizuguchi M, Ozawa H, Okazaki E, Kobayashi Y, Takahashi M, Ohtani K, Ogawa A, Narita M, Togashi T, Takashima S (2003). Apoptosis and microglial activation in influenza encephalopathy. *Acta Neuropathol* **105:** 233-9.

Newland J, Laurich V, Rosenquist A, Heydon K, Licht D, Keren R, Zaoutis T, Watson B, Hodinka R, Coffin S (2007). Neurologic complications in children hospitalized with influenza: characteristics, incidence, and risk factors. *J Pediatr* **150:** 306-10.

Nunoi H, Mercado M, Mizukami T, Okajima K, Morishima T, Sakata H, Nakayama S, Mori S, Hayashi M, Mori H, Kagimoto S, Kanegasaki S, Watanabe K, Adachi N, Endo F (2005). Apoptosis under hypercytokinemia is a possible pathogenesis in influenza-associated encephalopathy. *Pediatr Int* **47:** 175-9.

Okita K, Tokino T, Nishimori H, Miura K, Nikaido H, Hayakawa J, Ono A, Kuwajima M, Matsuzawa Y, Nakamura Y (1996). Definition of the locus responsible for systemic carnitine deficiency within a 1.6-cM region of mouse chromosome 11 by detailed linkage analysis. *Genomics* **33:** 289-91.

Olney J, Tenkova T, Dikranian K, Muglia L, Jermakowicz W, D'Sa C, Roth K (2002). Ethanol-induced caspase-3 activation in the in vivo developing mouse brain. *Neurobiol Dis* **9:** 205-19.

Papadopoulos M, Davies D, Moss R, Tighe D, Bennett E (2000). Pathophysiology of septic encephalopathy: a review. *Crit Care Med* **28:** 3019-24.

Paul R, Koedel U, Winkler F, Kieseier B, Fontana A, Kopf M, Hartung H, Pfister H (2003). Lack of IL-6 augments inflammatory response but decreases vascular permeability in bacterial meningitis. *Brain* **126:** 1873-82.

Pekny M, Eliasson C, Chien C, Kindblom L, Liem R, Hamberger A, Betsholtz C (1998). GFAP-deficient astrocytes are capable of stellation in vitro when cocultured with neurons and exhibit a reduced amount of intermediate filaments and an increased cell saturation density. *Exp Cell Res* **239:** 332-43.

Pekny M, Pekna M (2004). Astrocyte intermediate filaments in CNS pathologies and regeneration. *J Pathol* **204:** 428-37.

Petty M, Lo E (2002). Junctional complexes of the blood-brain barrier: permeability changes in neuroinflammation. *Prog Neurobiol* **68:** 311-23.

Rath P, Aggarwal B (1999). TNF-induced signaling in apoptosis. *J Clin Immunol* **19:** 350-64.

Reyes R, Guo M, Swann K, Shetgeri S, Sprague S, Jimenez D, Barone C, Ding Y (2009). Role of tumor necrosis factor-alpha and matrix metalloproteinase-9 in blood-brain barrier disruption after peripheral thermal injury in rats. *J Neurosurg*.

Schulze C, Smales C, Rubin L, Staddon J (1997). Lysophosphatidic acid increases tight junction permeability in cultured brain endothelial cells. *J Neurochem* **68:** 991-1000.

Smidt MH, Stroink H, Bruinenberg JFM, Peeters M (2004). Encephalopathy associated with influenza A. *European Journal of Paediatric Neurology* **8:** 257-260.

Starko K, Ray C, Dominguez L, Stromberg W, Woodall D (1980). Reye's syndrome and salicylate use. *Pediatrics* **66:** 859-64.

Stenvinkel P, Ketteler M, Johnson R, Lindholm B, Pecoits-Filho R, Riella M, Heimbürger O, Cederholm T, Girndt M (2005). IL-10, IL-6, and TNF-alpha: central factors in the altered cytokine network of uremia--the good, the bad, and the ugly. *Kidney Int* **67:** 1216-33.

Stolp H, Dziegielewska K, Ek C, Habgood M, Lane M, Potter A, Saunders N (2005). Breakdown of the blood-brain barrier to proteins in white matter of the developing brain following systemic inflammation. *Cell Tissue Res* **320:** 369-78.

Takahashi K, Sugi Y, Hosono A, Kaminogawa S (2009). Epigenetic regulation of TLR4 gene expression in intestinal epithelial cells for the maintenance of intestinal homeostasis. *J Immunol* **183:** 6522-9.

Takeda K, Akira S (2004). TLR signaling pathways. *Semin Immunol* **16:** 3-9.
Togashi T, Matsuzono Y, Narita M, Morishima T (2004). Influenza-associated acute encephalopathy in Japanese children in 1994-2002. *Virus Research* **103:** 75-78.

Takuma K, Baba A, Matsuda T (2004). Astrocyte apoptosis: implications for neuroprotection. *Prog Neurobiol* **72:** 111-27.

Toovey S (2008). Influenza-associated central nervous system dysfunction: a literature review. *Travel Med Infect Dis* **6:** 114-24.

Tsuda Y, Isoda N, Sakoda Y, Kida H (2009). Factors responsible for plaque formation of A/duck/Siberia/272/1998 (H13N6) influenza virus on MDCK cells. *Virus Res* **140:** 194-8.

Tsukita S, Furuse M, Itoh M (2001). Multifunctional strands in tight junctions. *Nat Rev Mol Cell Biol* **2:** 285-93.

Urayama A, Grubb J, Sly W, Banks W (2004). Developmentally regulated mannose 6-phosphate receptor-mediated transport of a lysosomal enzyme across the blood-brain barrier. *Proc Natl Acad Sci U S A* **101:** 12658-63.

Vezzani A, Balosso S, Ravizza T (2008). The role of cytokines in the pathophysiology of epilepsy. *Brain Behav Immun* **22:** 797-803.

Waldman R, Hall W, McGee H, Van Amburg G (1982). Aspirin as a risk factor in Reye's syndrome. *JAMA* **247:** 3089-94.

Wang L, Reinach P, Lu L (2005). TNF-alpha promotes cell survival through stimulation of K+ channel and NFkappaB activity in corneal epithelial cells. *Exp Cell Res* **311:** 39-48.

Weitkamp J, Spring M, Brogan T, Moses H, Bloch K, Wright P (2004). Influenza A virus-associated acute necrotizing encephalopathy in the United States. *Pediatr Infect Dis J* **23:** 259-63.

Wilson J, Young G (2003). Progress in clinical neurosciences: sepsis-associated encephalopathy: evolving concepts. *Can J Neurol Sci* **30:** 98-105.

Yao D, Chen Y, Kuwajima M, Shiota M, Kido H (2004). Accumulation of mini-plasmin in the cerebral capillaries causes vascular invasion of the murine brain by a pneumotropic influenza A virus: implications for influenza-associated encephalopathy. *Biol Chem* **385:** 487-92.

Yokota S, Imagawa T, Miyamae T, Ito S, Nakajima S, Nezu A, Mori M (2000). Hypothetical pathophysiology of acute encephalopathy and encephalitis related to influenza virus infection and hypothermia therapy. *Pediatr Int* **42:** 197-203.

Yuan J, Yankner B (2000). Apoptosis in the nervous system. *Nature* **407:** 802-9.

Zhou H, Andonegui G, Wong C, Kubes P (2009). Role of endothelial TLR4 for neutrophil recruitment into central nervous system microvessels in systemic inflammation. *J Immunol* **183:** 5244-50.

Acknowledgements

和文抄録

　　インフルエンザ脳症 (IAE) はインフルエンザウイルス感染に伴う致死的な中枢神経疾患の一つである。本邦では毎年 100 例前後の患者がみられ、5 歳以下の幼児での発生が全体の約 8 割を占めている。死亡率は約 30%と高く、神経学的後遺症が遺残することも多いため、効果的な治療・予防法の確立が急務である。本疾患の特徴的な臨床所見はインフルエンザによる発熱の直後に現れる左右対称性の急性脳浮腫で、その後しばしば播種性血管内凝固、多臓器不全の続発を伴うことがある。患者剖検例の病理組織学的検査では脳血管の障害による血液脳関門 (BBB) の破綻が明らかであるため、急性経過での血管障害が IAE の基盤病変であると考えられている。

　　本疾患の発症メカニズムに関しては解明されていない点が多く、動物モデルもこれまでに報告されていない。患者の中枢神経系からはインフルエンザウイルスが分離されないことから、ウイルス感染による直接的な脳組織傷害が本疾患の原因である可能性は低いと考えられる。一方、患者の血液中には TNF-α、IL-1β、IL-6 などの炎症性サイトカインの上昇が認められることが多い。これら炎症性サイトカインの血中濃度と IAE の重篤度が比例することから、サイトカイン血症による急性の血管障害が IAE の原因であるという説が有力である。

　　インフルエンザ脳症の病理組織学的所見がエンドトキセミアによる脳症と類似することから、本論文の第 1 章では、インフルエンザ A ウイルス (IAV) 感染乳のみマウスへのリポポリサッカライド (LPS) 投与による IAE モデルの作出を試みた。IAV と LPS を接種したマウス (IAV+LPS 群) では LPS 単独接種群

のマウスに比べ、神経病原性と脳血管透過性の亢進がより重度に発現すること
が分かった。病理組織学的検索では、IAV+LPS 群の脳に微小出血、浮腫および
好中球浸潤が認められ、同群マウスは IAE と同様の血管障害による脳症を示し
ていた。IAV+LPS 群マウスの血漿では、IAV または LPS を接種したマウスに比
べ、TNF-α、IL-6 が有意に上昇しており、IAE 患者の血清学的検査所見に一致し
ていた。また、IAV+LPS 群マウスの脳には IAV の感染は認められなかった。同
群マウスで観察された脳病変、血中サイトカイン動態、および脳における IAV
の不在が IAE の特徴に一致していたことから、IAV 感染乳のみマウスは LPS 接
種により IAE 類似脳症を示し、IAE の病態モデルとなることが明らかにされた。

　　　本論文の第 2 章では、IAV+LPS 接種マウスにおける IAE 様脳病変の形成
メカニズムを病理学的に解析した。その結果、IAV+LPS 群マウスの脳では IAV
または LPS 接種群と比べ、アポトーシス細胞の増加がみられた。アポトーシス
は主に脳の血管周囲で見られ、その一部は血管内皮様の紡錘形細胞だった。ま
た、アポトーシス陽性細胞の一部はアストロサイトのマーカーに対して陽性を
示した。アストロサイトと血管内皮細胞は BBB の機能と密接に関係しており、
IAV+LPS 群マウスでは、これらの細胞のアポトーシスによる BBB の破綻が IAE
様脳病変を引き起こす一因になっていることが示唆された。一方、脳血管内皮
細胞に発現するタイトジャンクション (TJ) 蛋白質の発現量を比較したところ、
マウス群間での有意な差は認められなかった。このことから、IAV+LPS 群マウ
スの IAE 様脳症の形成には TJ の機能低下による内皮細胞間透過性の亢進は重要
な要因ではないと考えられた。過去の報告によると、IAE 患者の脳グリア細胞や
血管内皮細胞においてもアポトーシスの増加が示されており、本実験の

IAV+LPS 群マウスの脳症病変は IAE と共通のメカニズムにより形成されていることが示唆された。

　　　本論文では、乳のみマウスにおいて IAV の肺感染が LPS 誘発性の脳症および炎症性サイトカイン産生を増強させることを示した。同処置を行ったマウスの脳の病理組織像、血中サイトカイン動態およびウイルス分布は IAE の特徴に一致した。また、その脳症病変の形成には脳血管内皮細胞とアストロサイトのアポトーシスが関与しており、本実験の IAV+LPS マウスでは IAE と共通のメカニズムにより脳症病変が形成されていると考えられた。また、IAV+LPS 群マウスでは血中サイトカイン濃度の上昇が脳におけるアポトーシス誘導の引き金となっていると考えられ、ヒトにおいても高サイトカイン血症による脳血管内皮細胞とアストロサイトのアポトーシスがIAEの原因となる可能性が示された。本マウスモデルは IAE の早期診断法と有効な治療法の開発に役立つことが期待される。